Graduate Theses and Dissertations   Graduate School

January 2013

Novel Approach of Using Polyvinylidene Fluoride Langmuir-Schaefer Film on Graphene-Polyaniline Nanocomposite for Supercapacitor Applications

Venkata Priyanka Bolisetty
University of South Florida, piya.vaishu@gmail.com

Novel Approach of Using Polyvinylidene Fluoride Langmuir-Schaefer Film on

Graphene-Polyaniline Nanocomposite for Supercapacitor Applications

by

Venkata Priyanka Bolisetty

A thesis submitted in partial fulfillment
of the requirements for the degree of
Master of Science in Electrical Engineering
Department of Electrical Engineering
College of Engineering
University of South Florida

Co-Major Professor: Manoj K. Ram, Ph.D.
Co-Major Professor: Arash Takshi, Ph.D.
Lee Stefanakos, Ph.D.
Yogi Goswami, Ph.D.
Sylvia Thomas, Ph.D.

Date of Approval:
March 25, 2013

Keywords: Polymer materials, electrochemical, Langmuir Blodgett, dielectric constant, leakage current, conducting polymer

DEDICATION

My thesis work is dedicated to my parents who have given a lot of support and always been a part in my each endeavor. My parents are always my source of inspiration; always they encourage me to do special things in my life. Similarly, my sister and brother are always there to help, love and care for my effort and I always owe to them. Finally, I am always grateful to my all friends and well-wishers who are supportive throughout in preparation of my master thesis.

TABLE OF CONTENTS

LIST OF TABLES

LIST OF FIGURES

ABSTRACT

Supercapacitors are well known for their improvised power density compared to batteries. Ongoing research is mainly focused on improving the energy density of supercapacitors by using different electrode material nanocomposites. The recent research has revealed that graphene (G)-polyaniline (PANI) nanocomposite could be a promising material for supercapacitor applications. The supercapacitor is also associated with self-leakage current regardless of any electrode material. The main objectives of the project are to: (i) synthesize highly fabricate supercapacitor based of G-PANI electrode; (ii) improve the energy density of supercapacitor by applying ultrathin monolayer/monolayers film electrode surface. It is crucial to either improve or retain the effective capacitance of the dielectric film. The dielectric material chosen is polyvinylidene fluoride (PVDF) due to its dielectric constant and electrochemical properties. Langmuir-Schaefer (LS) technique is used to deposit the PVDF film onto the substrate. The optical properties of electrode materials were measured by UV-vis spectrophotometer. The surface morphology of the fabricated electrode material has been investigated using scanning electron microscopic (SEM) and atomic force microscopic (AFM) studies. The supercapacitor with and without dielectric layer have been studied using cyclic voltammetry, charging and discharging, and electrochemical impedance techniques, respectively. The specific capacitance has been found to increase by application of one monolayer of PVDF film of G-PANI electrode. However, the LS film of PVDF does not show the minimization of leakage current but revealed an increase in

the specific capacitance due to enhancement in surface area associated with the electrode besides PVDF is also an electrochemical active material. The electrochemical investigation of various layers of PVDF on G-PANI in symmetric and asymmetric supercapacitor configuration has been presented in thesis. The future scope of the project could be designing the electrode with various number of layers of dielectric material that could reduce the leakage current, and retaining the specific capacitance of G-PANI nanocomposite electrodes**.**

CHAPTER 1: OVERVIEW OF SUPERCAPACITORS

1.1 Introduction: Supercapacitors

The need for energy resources is increasing day by day in the present world. Fossil fuels and batteries served the purpose for many years, and the increase in demand resulted in high cost of materials and depletion of natural resources [1-5]. Alternate energy is very essential to satisfy the present crisis in the world. Supercapacitors are energy storage devices that work based on the principle of double layer capacitance and pseudocapacitance. They serve the purpose for alternate energy due to their low cost and environmental friendliness [6-10]. Electrochemical capacitors (ECs) also known as supercapacitors or ultra-capacitors are well known for their improvised power density compared to batteries [11-14]. The main advantages are higher power density, hence quick charging and discharging without much degrading unlike batteries, recycle capability, less toxic, environmental friendly, low cost, operate over wider temperature ranges, very light weight compared to batteries and fuel cells [15-17]. Some disadvantages include high self-discharge rate, lower energy density compared to batteries and fuel cells, lower cell voltage and poor voltage regulation. They find extensive usage in hybrid vehicle cars, power supplies, generators, inverters, load leveling, electricity storage, etc. [1]. The usage of capacitors includes coupling alternate current (AC) and direct current (DC). The ability of high power density is useful in filtering, backup and timer circuits. Capability of blocking DC is used in filters [2]. The

ECs do not possess high energy density unlike the batteries. Ongoing research is mainly based on improving the energy density by enhancing the material properties. Enhancing the performance of supercapacitors emphasizes on longer life cycle, extension in rated voltage, voltage range improvements in operating temperature, improvement in energy and power density and decrease in self-leakage current.

The aim of the present work is based on understanding the application of monolayer/multilayers PVDF dielectric layer over G-PANI electrode for supercapacitor applications. The increase of specific capacitance with application of one monolayer PVDF dielectric layer shows a way to enhance the performance of supercapacitors for practical applications. The thesis also presents the experimental findings of various applications of LS films on supercapacitor properties of the G-PANI based electrodes.

1.2 Types of Capacitors

Electrostatic capacitors contain two electrical conductors separated by a dielectric media. Capacitance is in the range 1 pF to 1μF with a voltage range of (50V to 400V). Electrolytic capacitors are the aluminum and tantalum capacitors where solid/ liquid electrolytes are used with a separator between the electrodes [3]. Capacitance lies in the range 0.1 to 10000 μF with a voltage range of (16V to 50V). Electric Double Layer Capacitors (EDLCs) are the carbon based electrode materials. They could store charge up to 10^6 Farads [2].
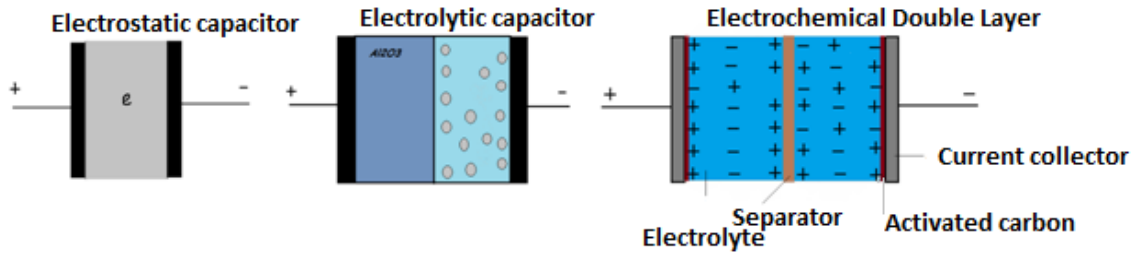
Figure 1: Schematic sketch of electrostatic capacitor, electrolytic capacitor and electrical double layer capacitor [2]

A capacitor is a device which stores energy in an electric field. It mainly consists of two electrode plates separated by a dielectric medium. When some voltage is applied across the plates, charges are accumulated on the electrodes causing an electric field to be generated in between the plates, which makes the capacitor to store energy [4]. The capacitance C is given by:

$$C = \frac{Q}{V} \tag{1}$$

where, C = capacitance, Q = charge accumulation across the plates, and V = voltage applied to the capacitor.

The capacitance of the parallel plate capacitors is given by:

$$C = \epsilon_0 \epsilon_r \frac{A}{D} \tag{2}$$

where, ε_0 = permittivity of free space, ε_r = permittivity of dielectric layer in between the electrodes, A = area of the electrodes, and D = distance between the electrodes.

The performance of a capacitor can best be known by finding the power density and energy density.

3

Energy density is given by:

$$E = \frac{1}{2}CV^2 \tag{3}$$

and power density is given by:

$$P = \frac{V^2}{4ESR} \tag{4}$$

where, ESR is the equivalent series resistance. ESR is primarily responsible for limiting the maximum power of the supercapacitor.

The power loss during charge or discharge process is calculated using

$$P_{loss} = I^2.ESR \tag{5}$$

Conventional capacitors have higher power density (<100,000 W/kg) and lower energy density (<0.1 Wh/kg) i.e. they charge and discharge very rapidly, but store less energy compared to batteries and fuel cells. Electrochemical capacitors have higher energy density but lower power density in comparison to conventional capacitors [5]. This can best be shown in the Ragone Plot [6].
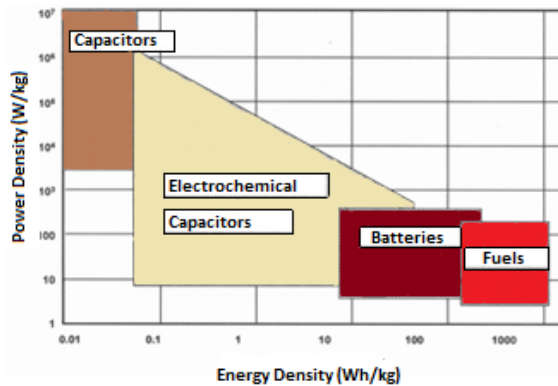
Figure 2: Ragone plot for different energy storage devices (modified [6])

1.3 Supercapacitor Mechanism

Supercapacitors generally consist of a carbon based electrode material. The electrode material can be carbon nanotubes (CNTs), multi-walled-carbon nanotubes (MWCNTs), metal oxides or polymer nanocomposites. Supercapacitor term is coined for electric double layer capacitor. When an electric charge is applied to the electrode, positive ions and negative ions get attracted to opposite charges on both the electrodes. This creates a thin molecule size double layer which acts as a parallel plate capacitor with dielectric in between them. When sufficient voltage is applied, the current begins to flow to charge the capacitor.
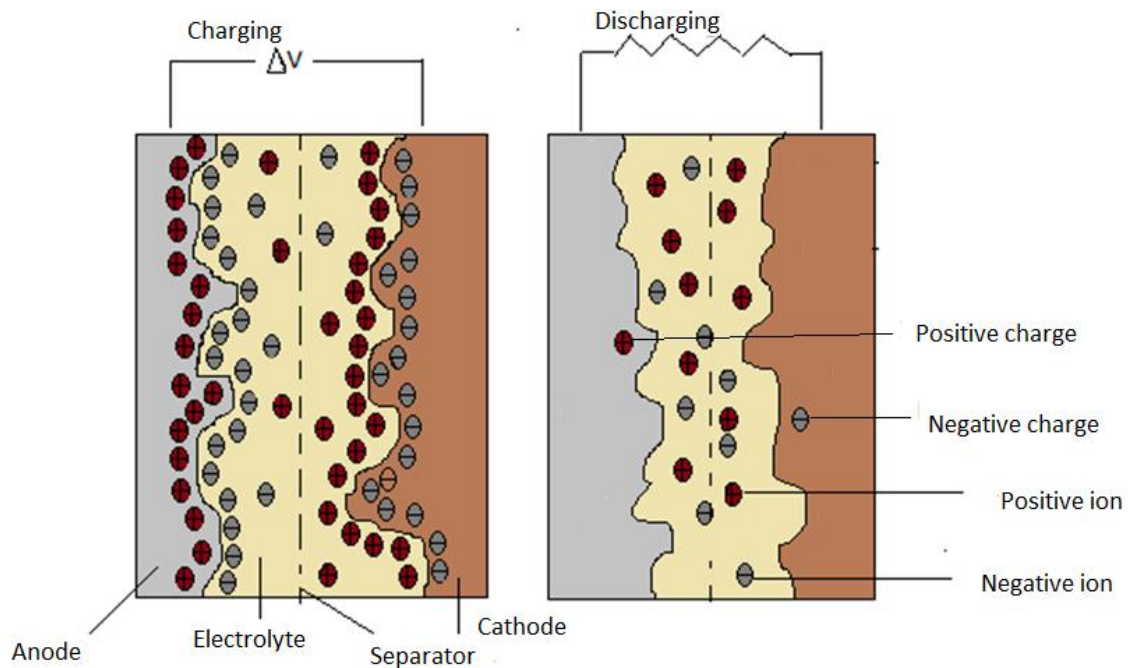
Figure 3: Schematic sketch of a supercapacitor during charging and discharging mode

Typical charging and discharging states are shown in the above figure (3) [7]. Performance of a supercapacitor is based on two mechanisms: non faradic charge storage

5

and faradic charge storage. Electric double layer capacitors (EDLCs) store electric charge at the electrode/electrolyte interface i.e. non faradic charge storage which is due to attraction of opposite charges on the electrode surface forming a thin double layer of electrostatic charges. The associated capacitance is called double layer capacitance. Carbon based materials exhibit this behavior due to no chemical or compositional changes associated during charging or discharging. Electrochemical double layer capacitors or pseudocapacitors sustain faradic reaction or redox processes with electro-sorption or intercalation (doping/dedoping) that takes place at the electrolyte/electrode interface. Supercapacitors can be made of incorporating both carbon based materials and pseudocapacitive materials such as conducting polymers to form carbon based conducting polymer nanocomposites. Such mechanism can have faradic and non faradic charge storage. The electrode material can consists of transition metal oxides, carbon based materials, polymer based materials, and metal oxides/polymer based carbon composites. The associated capacitance is pseudocapacitance along with double layer capacitance. Pseudocapacitance is responsible for faradic reactions that take place at the interface.

The capacitance value changes with concentration and type of electrolyte (aqueous or organic based) used for cell configuration. The specific capacitance of most carbon based electrodes in organic electrolytes is less compared to the ones in aqueous electrolytes. This is due to low dielectric constant of organic electrolytes which leads to low energy density [1]. An advantage of using organic electrolytes is they give wider operating voltage window compared to aqueous electrolytes [1]. Typical construction of an EDLC

is shown in the figure (4) [8]. Specific capacitance of a supercapacitor is directly proportional to the specific area.
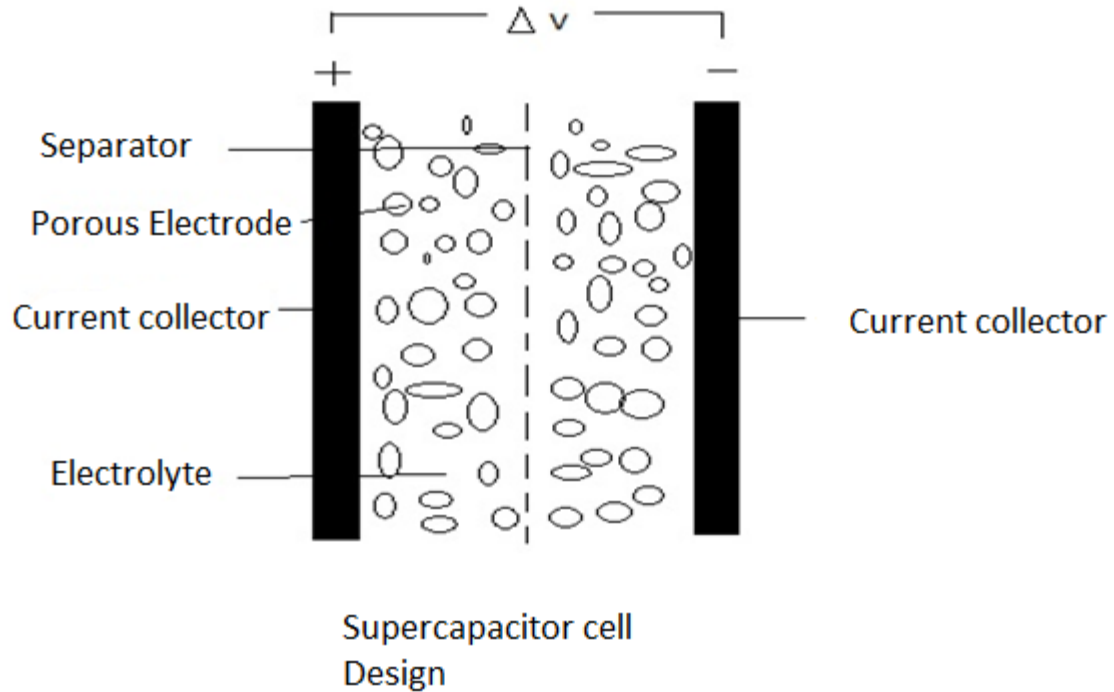
Figure 4: Schematic sketch of an electrical double layer capacitor

There are other factors like structure of carbon, pore size, size of the particle, conductivity associated with the electrolyte and some surface functionality which influence capacitance [2],[5]. The reason for development of pseudocapacitors exhibiting faradic charge storage mechanism is because double layer capacitors exhibit lower charge storage in comparison to pseudocapacitors, hence low capacitance per unit surface area. There is a high need for improvement in energy storage leading to the development of hybrid capacitors. They include both double layer capacitance and pseudocapacitance resulting in higher capacitance output.

1.4 Self-Discharge and Leakage Current

The self-discharge in a supercapacitor is important for the use of the device in long term electrochemical energy storage system [4]. The self-discharge in a supercapacitor is due to faradic redox reactions that take place at the electrode/electrolyte interface when the electrical supply is disconnected [4]. Self-discharge or leakage current minimization is important for the applications of a supercapacitor as an energy storage device [9]. The application requires that the device be able to deliver power with a performance but not degrading with time. The leakage current also causes the voltage drop with time of a charged capacitor at open circuit potential [3]. The leakage current is linked to faradic redox reactions, ionic charge diffusion or/and electronic partial discharge through the separator [10]. The self-discharge is determined by measuring the current required to maintain a constant voltage, or by measuring the capacitor voltage with change in time [3]. According to the voltage-time dependency, if the voltage drops with logarithmic law, the mechanisms are under control by faradic self-discharge either from overcharge or due to redox reactions of impurities presents in the anode or cathode electrode materials [10]. If the voltage drops with the square of time, the mechanism is due to control of diffusion processes at the electrode/electrolyte interface [10]. The leakage current of the supercapacitor increases with the increase of temperature and results in compromising the power capability of the device [9].
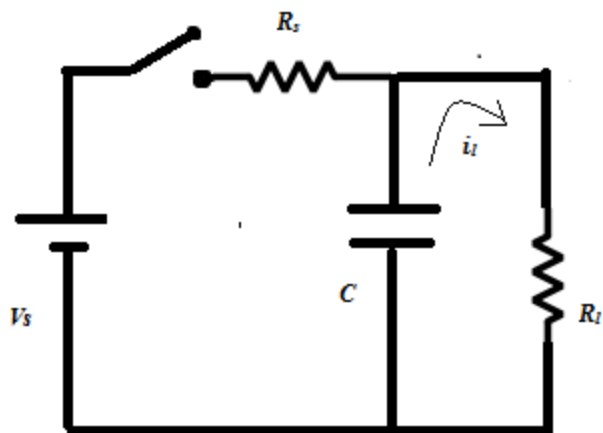
Figure 5: Equivalent circuit for self-discharge

The circuit in figure (5) describes the leakage current associated with the electrode material at open circuit potential [3],[11]. V_s= voltage source, R_s= series resistance, C= capacitance, R_l= leakage resistance. The leakage resistance associated is not constant; it changes with voltage and properties of the electrode material [12]. For a pseudocapacitor, it changes with redox reactions that occur at the electrode interface which may react with the electrode or electrolyte [13]. Leakage current is measured by charging the capacitor to a fixed voltage and measuring the change in potential with respect to time at open circuit potential of the capacitor during self-discharge [3],[14]. The leakage current is inversely proportional to leakage resistance, the more the leakage resistance the less the leakage current. Applying an interfacial dielectric layer on top of the electrode material changes the kinetic rate at which electrochemical reactions occur at the electrode/electrolyte interface. On application of dielectric layer, the kinetic rate decreases leading to a drop in leakage current. Hence, the insulating layer can be modeled as larger resistance.

9

1.5 Supercapacitor Electrode Materials

The specific energy below 10 Wh/kg for carbon based EDLCs , 35-40 Wh/kg for batteries (lead acid based) and 150 Wh/kg for lithium ion batteries [2] are available in literature. There is a need for improving the energy density of the supercapacitors so that it could take the place of batteries. Lot of ongoing research is based on synthesis of different electrode materials and analysis of their capacitive behavior using different electrolytes. Over the years, cost per Farad kept on decreasing which shows significant improvement in commercially available supercapacitors [15]. Table 1 gives the cost analysis of supercapacitors [15]. Table 2 provides significant differences between various energy storage systems [16].

Table 1: Cost trend of supercapacitors [15]

Year	Cost/Farad ($)	Cost /kJ($)
1996	0.75	281.55
1998	0.4	151.23
2000	0.01	32
2002	0.023	7.51
2006	0.01	2.85
2010	0.005	1.28

Table 2: Comparison of conventional storage devices [16]

Performance	Lead acid Battery	Supercapacitor	Conventional Capacitor
The charging time	1 - 5 hours	0.3 - 30 sec	10^{-3} - 10^{-6}
The discharging time	0.3 - 3 hours	0.3 - 30 s	10^{-3} - 10^{-6}
Energy in Wh/kg	10 -100	1 - 10	< 0.1
The cycle life	1000	> 500,000	> 500,000
Specific power (W/kg)	< 1000	< 10,000	< 100,000
Charge /discharge efficiency	0.7 - 0.85	0.85 - 0.98	> 0.95

Table 3 shows various characteristics in comparison between Lithium ion batteries and electrochemical capacitors [17].

Table 3: Differences between lithium ion battery and electrochemical capacitor [17]

Characteristics	Lithium Ion Battery	Electrochemical Capacitor
[1]Charge Time	~3-5 minutes	~1 second
Cycle Life	<5,000 @1C rate	>500,000
Specific Energy (Wh/kg)	70-100	5
Specific Power (kW/kg)	[2]0.5-1	5 to 10
Cycle Efficiency	<50% to > 90 %	<75 to > 95 %
Cost/Wh	$1-2/Wh	$10-20/Wh
Cost/kW	$75-150/kW	$25-50/kW

[1] It is the time taken for discharge and charge of the useable total energy stored in the devices

[2] It is the power capability of the battery for short duration partial at 90% efficiency
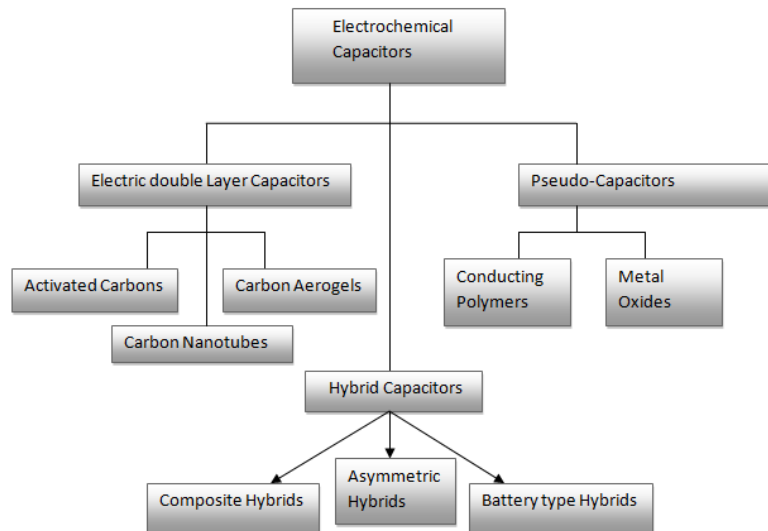
Figure 6: Taxonomy of supercapacitors

As discussed earlier, different types of electrochemical capacitors [18] include double layer capacitors and pseudocapacitors. The double layer capacitors based on carbon materials are carbon nanotubes (CNTs) and activated carbons which exhibit high specific area and low mass density. The different forms of nanotubes such as single-walled and multi-walled allow high accessibility of electrolyte due to their surface morphology, high surface area and extreme good mechanical properties [19]. The conducting polymers and metal oxides exhibit pseudocapacitance due to their redox properties giving high specific capacitance values. Hybrid capacitors are formed by incorporating conducting polymers into carbon based compounds using various techniques, thereby improving the device performance in terms of conductivity, stability and specific energy density. Composite hybrids include two different types of electrode materials forming nanocomposites, enhancing the capacitor performance. Asymmetric type hybrids are constructed with two different types of nanocomposites for anode and cathode. This configuration makes use of operating voltages of each material. High stability devices can be configured using such method [5]. Battery type hybrids make extensive usage where energy density and power density is of high importance. The overall performance in both the terms can be improved using such design compared to individual single components [1].

Table 4 [20] provides useful information regarding operating voltage and specific capacitance values of each different electrode material in different electrolytes. We could see that the conducting polymers exhibit better specific capacitance values compared to carbon based composites which is due to the effect of pseudocapacitance. Transition metal oxides show relatively higher capacitance values, but since they are rare earth metals, they are expensive and are not readily available [20].

12

Table 4: List of specific capacitance values for various types of electrode materials [20]

	Electrode Material	Electrolyte	Working Voltage(V)	Specific Capacitance (F/g)
Carbon based	Activated carbon (AC)	1 M Et_4NBF_4 + PC	1.5	40
	Graphite	1 M Et_4NBF_4 + PC	3	12
	carbon aerogels(CAGs)	1.5 M Et_3MeNBF_4 + PC	3	160
	Mesoporous carbon	30 wt% KOH	0.9	180
	Meso/macroporous carbon	6M KOH	0.8	130
	C_{60}-loaded AC fiber	0.5 M H_2SO_4	1	172
	AC fiber cloth	6 M KOH	1	208
	Single-walled-CNTs	EMITFSI	2.3	50
	Multi-walled CNTs sheet	1.96 M TEMABF$_4$ +PC	2.5	13
	CNTs/polypyrrole(ppy)/MnO_2	1 M Na_2SO_4	0.9	281
Transition metal oxide	$RuO_2.H_2O$	0.5 M H_2SO_4	1	650
	Ruthenic acid nanosheet/Au	0.5 M H_2SO_4	1.2	620
	$H_{0.2}RuO_{2.1}.nH_2O$	0.5 M H_2SO_4	1.2	390
	RuO_2/carbon	PVA hydrogel	0.8	1000
	Amorphous $Ru_{1-y}Cr_yO_2$/TiO_2	1 M KOH	0.9	1272
	MnO_2	0.5 M K_2SO_4	0.8	261
	MnO_2/AC	0.65 M K_2SO_4	2.2	29
	SnO_2/carbon aerogel	1 M H_2SO_4	1	68
	$Ni(OH)_2$	3% KOH	0.8	578
	$Ni(OH)_2$/AC	6 M KOH	0.9	194
	cobalt-nickel oxides/CNTs	1M KOH	1	569
	Nickel-based mischmetal/AC	BMIM-PF_6	3	357
	Mo_2N/Ta_2O_5	3.5 M H_2SO_4	0.8	106
	WC/carbon	1 M H_2SO_4	0.9	477
	$MnFe_2O_4$	1 M $LiPF_6$ + EC/EMC	2.5	126
	TiN	1M KOH	0.2	238
	V_2O_5	2M KCl	0.7	262
Conductive polymers	Poly(3-methylthiophene)	$PYR_{14}TFSI$	3.6	25
	poly(3-methylthiophene)/MnO_2	1 M Na_2SO_4	1	381
	polypyrrole/AC	0.5 M pyrrole+0.5M β-NSA	0.9	345
	PANI/MnO_2	0.1 M Na_2SO_4	1.2	715
	PANI/AC	6M KOH	0.9	588

A lot of research is being done to improve the specific capacitance values of electrode materials of conducting polymers by incorporating them with carbon based materials forming nanocomposites.

Expansions of acronyms listed above: Tetraethylammonium tetrafluroborate (Et_4NBF_4), propylene carbonate (PC), triethyl methyl ammonium tetrafluoroborate (Et_3MeNBF_4), potassium hydroxide (KOH), sulphuric acid(H_2SO_4), 1-ethyl-3-methylimidazolium bis-(trifluoromethylsulfonyl)-imide (EMITFSI), triethylmethylammonium tetrafluoroborate (TEMABF$_4$), sodium sulphate (Na_2SO_4), ruthenium dioxide (RuO_2), polyvinyl alcohol (PVA), manganese dioxide (MnO_2), tin dioxide(SnO_2), nickel hydroxide ($Ni(OH)_2$), gold (Au), potassium sulphate (K_2SO_4), 1-butyle-3-methylimidazolium hexafluorophosphate (BMIM-PF$_6$), molybdenum nitride (Mo_2N), tantalum pentoxide (Ta_2O_5), tungstun carbide/carbon (WC/carbon), manganese ferrite($MnFe_2O_4$), lithium hexafluro phosphate (LiPF$_6$), ethyl carbonate (EC), ethylene methyl carbonate (EMC), titanium nitride (TiN), vanadium pentoxide (V_2O_5), 1-butyl-1-methylpyrrolidinium bis(trifluoromethanesulfonyl (PYR$_{14}$TFSI), naphthalene sulphonic acid (β-NSA).

1.6 Electrochemical Measurements and Methods

1.6.1 Cell Configuration

An electrochemical cell setup to analyze the capacitive behavior of any electrode material generally consists of either two electrode system or three electrode system. A two electrode cell setup consists of two electrodes of same type are connected in series connection with electrolyte solution in between them. Three electrodes cell setup contains the working electrode with electrode material for capacitance evaluation, counter

electrode such as platinum wire or mesh, and reference electrode. The capacitance has been examined using three electrode system. In case of a series connection of a two electrode system, the overall capacitance would be half of the individual capacitances due to the reciprocal relationship as shown in figure(7) [21].

$$\frac{1}{C} = \frac{1}{C_1} + \frac{1}{C_2}$$

(6)

Figure 7: Simplified equivalent circuit of a two electrode system

1.6.2 Cyclic Voltammetry (CV)

The CV shows the potential window in the plot of current vs. potential. The potential is scanned from a certain initial voltage to a certain final potential to charge the supercapacitor and again scanned back in the reverse direction to discharge it. The resulting current density is plotted against potential with respect to reference electrode. The voltage limits are designed based upon the electrolyte decomposition limits [3],[5]. It can also be used to estimate the cycle life of the supercapacitor. The CV curve of an electric double layer capacitor would be a rectangular shape, in absence of faradic reaction. In presence of faradic redox reactions, the CV curve said to have peak currents which are due to the effect of pseudocapacitance exhibited by the electrode material.

15

The capacitance is calculated using

$$C = \frac{I_p}{v_s} \qquad (7)$$

where, I_p = peak current and v_s = scan rate applied.

Diffusion coefficient is calculated using the Randles-Sevcik equation i.e.

$$I_p = (269000)n^{3/2}ACD^{1/2}v^{1/2} \qquad (8)$$

where, i_p = peak current, n = number of electrons involved in the faradic redox reaction, A = area of the electrode (cm^2), C = concentration of the electrolyte (mol/cm^3), D = diffusion coefficient, v = voltage scan rate (mV/sec) [22]. This equation gives insight of the peak current depending not only on concentration and diffusion properties of the electrochemical active species but also on the value of scan rate. It is directly proportional to the electrolyte concentration and square root of the scan rate.

1.6.3 Charge-Discharge Method: Chronopotentiometry

On applying constant current to electrode material in contact with the solution electrolyte, there is some potential difference developed linearly with time [23]. The specific discharge capacitance can be calculated for electric double layer capacitor using the below equation

$$C = I\frac{T_2 - T_1}{V_2 - V_1} \qquad (9)$$

where, I = discharge current, T_1 = time where discharging starts, T_2 = time where discharging ends, V_1 = voltage at start of discharge, V_2 = voltage at end of discharge.

1.6.4 Self Leakage Measurement

Self leakage current is dependent on the leakage resistance associated with electrode material. The low leakage resistance results in high self leakage current. The electrode material is made to charge for a longer time with definite amount of current for it to reach the maximum potential (rated voltage), and then it is made to discharge with zero current for certain number of hours. The drift in voltage is due to the internal leakage current. The leakage current can be calculated by multiplying the capacitance value with the change in voltage across the time [3]. The more the leakage current, the more the loss in energy and power density coupled with the supercapacitor. So, there should be much importance on how to reduce the leakage current [23].

1.6.5 Electrochemical Impedance Spectroscopy (EIS)

The ideal impedance |Z$_c$| is useful in determining the capacitance of the supercapacitor.

$$|Z_c| = \frac{1}{2\pi f C} \tag{10}$$

EIS gives valuable information on solution resistance, double layer capacitance, electrode kinetics (charge transfer behavior) and diffusion control processes [24]. A Nyquist plot is very useful in analyzing and measuring the solution resistance and the polarization resistance. A Bode plot is used to see how impedance is changing with respect to the frequency. It can be used to calculate the apparent capacitance at any specific frequency.

(a)   *(b)*

Figure 8: (a) Randle's circuit model, (b) Randle's circuit model with constant phase element

The figure 8(a) represents the Randle's model with R_L = leakage resistance, C as ideal capacitance, ESR = series resistance (solution resistance) [11]. It is used to model a double layer capacitor. The leakage resistance or the polarization resistance is the combination of charge transfer resistance (R_{ct}) and the Warburg impedance (W) [25] . The straight line at low frequencies corresponds to the diffusion process occurring at the electrode/electrolyte interface and is called as the Warburg impedance. The equivalent circuit describing phase constant model as shown in figure 8(b) comprises the solution resistance (R_s), double layer capacitance (C_{dl}) , leakage resistance (R_L) , charge transfer resistance (R_{ct}) and Q (phase constant element). It is used to model a supercapacitor exhibiting double layer capacitance along with pseudocapacitance.

A nanocomposite of high energy density and surface area is considered to be an effective electrode material for enhancing performance of a supercapacitor. Recent research revealed (G-PANI) nanocomposite to be an excellent electrode material to be explored in terms of specific capacitance, energy and power density values. The G-PANI has been synthesized and the supercapacitor has been fabricated and studied. The Langmuir-monolayer/multilayers of thin dielectric film of PVDF is studied in the next chapters.

CHAPTER 2: ELECTRODE MATERIALS

2.1 Graphene and Conducting Polymers

Graphene is an allotrope of carbon with sp^2 bonded structure in the form of a honey comb lattice. The unique surface morphology of arrangement of 2D carbon atoms of a single layer results in very high surface area [26]. This property makes it a suitable material for electrochemical double layer capacitor fabrication. The graphene exhibits specific capacitance of about 100~200 F/g , energy density of 28.5 Wh/kg and power density of 10 kW/kg in aqueous electrolytes [27]. The surface area of about 2630 m^2/g is seen for graphene as an electrode material [28]. This makes it very different from EDLC's developed from activated carbons [5]. Graphene is said to exhibit very high chemical stability, mechanical strength, higher electrical conductivity and thermal conductivity [26]. Further, graphene can be used along with other pseudocapacitive materials such as conducting polymers and metal oxides that exhibit good energy density values to form graphene based nanocomposites that contribute to very high and improved energy densities [5]. They give rise to very high surface areas. The graphene with conducting polymer is easy to synthesize and can be done in bulk using oxidative polymerization [7]. The graphene-conducting polymers exhibit superior chemical stability with high rate of charge-discharge processes at the electrode surface, and exhibit a wider electrochemical window. They are low cost materials and produce environmental friendly energy storage devices. Metal oxides are another type of pseudocapacitive materials where graphene can

be incorporated to enhance the specific capacitance values. Extensive research was done on RuO_2 based metal oxide. The high specific capacitance of 720-900 F/g are shown in RuO_2 based material. Since it is expensive, the main usage is in military and aerospace applications. One other such metal oxide is IrO_2. Rarity of this metal oxide made researchers to focus on other transition metal oxides such as nickel(II) oxide (NiO), nickel(II) hydroxide ($Ni(OH)_2$), manganese dioxide (MnO_2), cobalt(III) oxide (Co_2O_3), iridium(IV) oxide (IrO_2), ferrous oxide (FeO_2), titanium dioxide (TiO_2), tin dioxide (SnO_2), vanadium pentaoxide (V_2O_5) and molybdenum dioxide (MoO_2). These are still under lab scale analysis. MnO_2 thin film supercapacitors exhibited 600 F/g [2]. Lot of research is focused on just metal oxide, or making a composite of metal oxide along with graphene, or mixing of two metal oxides with graphene. Conducting polymers include PPy, PANI, PEDOT and their derivatives are very efficient pseudocapacitive materials owing to their high redox properties and high doping levels. They are easy to synthesize, are low cost and have higher electrical conductivity allowing them to be extensively used in electrochemical capacitors [5]. They can be synthesized by oxidative polymerization or electrochemical deposition. In order to improve the energy density and to decrease the mechanical stress, carbon based materials are incorporated in conducting polymers. A specific capacitance of about 380 F/g has been reported for G-PEDOT. It is said to show columbic efficiency of about 95% for 800 cycles, suggesting remarkable stability in the composite [29]. A specific discharge capacitance of about 154 F/g is observed for graphene (G)-polythiophene (PTh) nanocomposite in different electrolytes with faster discharge rates allowing it to be an ideal supercapacitor electrode material [30]. Specific discharge capacitance in 2M HCl for G-PEDOT and G-PTh were estimated to be around

160 F/g to 400 F/g making them very suitable electrode materials for supercapacitor applications [31]. A different approach of grafted polyaniline nanofibers onto graphene forming a PANI-G hybrid exhibited specific capacitance of 623.1 F/g at a current density of 0.3 A/g [32]. Graphene with polyaniline and its derivatives such as graphene-poly (o-anisidine) (G-POA) and graphene-poly (o-toluidine) (G-POT) exhibited specific capacitances of about 400 F/g, 380 F/g and 425 F/g, respectively. These nanocomposites are said to be considered effective and safe electrode materials for supercapacitor applications [33],[34]. Graphene incorporated with polyaniline is said to exhibit better specific capacitance as high as 1046 F/g in 6M KOH [35]. G-PANI exhibited specific capacitance as high as 400 F/g [36],[37],[38] in aqueous electrolytes. It is very important to understand the different forms of PANI existence in order to have better knowledge of its conducting behavior. The PANI has four different redox states depending upon the applied potential. The PANI is in reduced state leucoemeraldine form (-0.2 V), emeraldine base and emeraldine salt (0.4 to 0.6V) and pernigraniline form (>0.8V). The figure (9) shows the protonated and deprotonated pernigraniline, protonated and deprotonated emeraldine, protonated and deprotonated leucoemeraldine form of polyaniline. It is possible to change one protonated to deprotonated states by giving or taking the two protons ($2H^+$) and two electrons ($2e^-$), respectively.
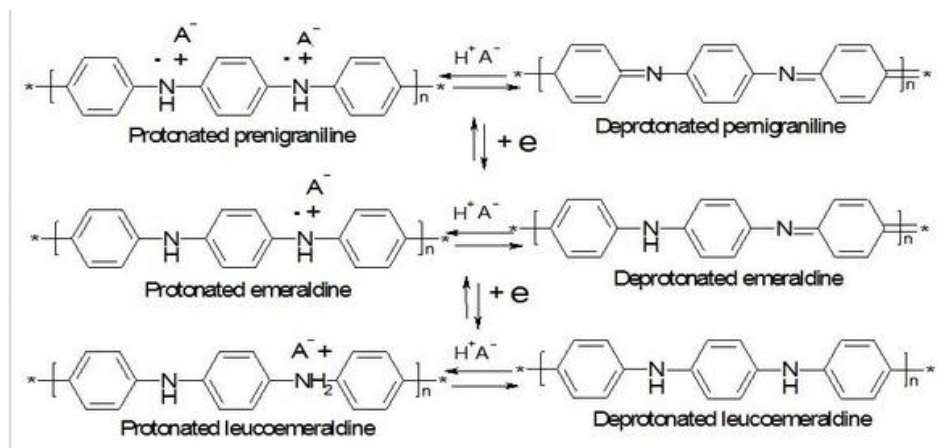
Figure 9: Different oxidation and reduction states of PANI (Reprinted with permission from [39])

The figure (9) describes different oxidation and reduction states of polyaniline conducting polymer [39].

Practical applications include reducing the leakage current with the application of a dielectric layer on top of the nanocomposite material. This ensures a potential barrier to decrease the rate of reaction. One such dielectric material is Barium Strontium Titanate (BST), which can be deposited using sputtering, is used for reducing the self leakage effect [40],[41]. The issue of leakage current is addressed by depositing a high dielectric film using the Langmuir Blodgett technique. The novel approach of using a ferroelectric polymer such as polyvinylidene fluoride (PVDF) with a very high dielectric constant of about (8-9.5) is used to reduce the self-leakage current, at the same time due to dipole alignment of the PVDF structure , there might be an increase in surface area resulting in high specific capacitance.

2.2 Polyvinylidene Fluoride (PVDF)

PVDF is a ferroelectric polymer which exhibits piezoelectric and pyroelectric properties [42]. Ferroelectric materials possess both piezoelectric and pyroelectric properties and they exhibit sudden switching in electric polarization on application of electric field [43]. These are very useful in sensor applications such as acoustic transducers, electromechanical actuators, heat sensors, etc. [44]. The strength of the electric dipoles of a ferroelectric material depends on material lattice structure [45]. Any change in the lattice results in change of dipole polarization, which changes the surface charge [45]. Force and temperature can change the lattice dimensions resulting in generation of surface charge, such changes correspond to piezoelectric and pyroelectric properties respectively [46]. The molecular formula of PVDF is $(CH_2CF_2)_n$ with molecular weight of 64.022 gram/mol [47]. PVDF exhibits two phases in material lattice 1) alpha phase 2) beta phase [48]. Figure 10 (b) and (c) shows the alpha and beta phases of PVDF.

(a)   (b)   (c)
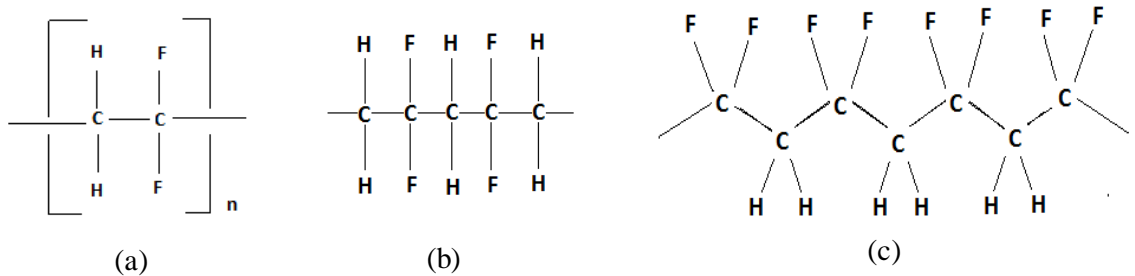
Figure 10: (a) Molecular structure of PVDF, (b) Alpha phase of PVDF, (c) Beta phase of PVDF
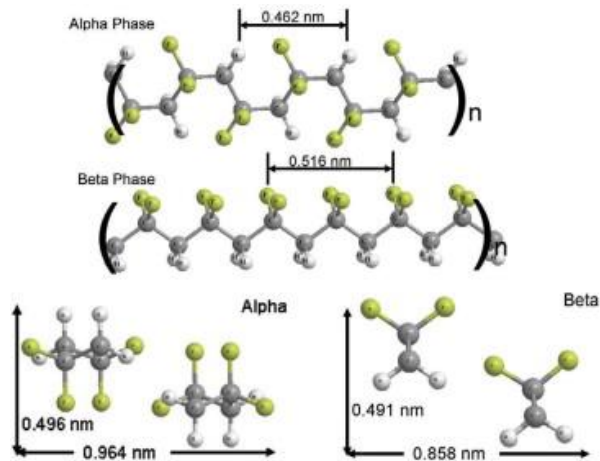
Figure 11: 3D view of PVDF molecules (Reprinted with permission from [49])

The figure (11) represents the 3-dimensional view of the PVDF molecules in alpha and beta phase [49]. Alpha phase is the initial phase, and using Langmuir Blodgett (LB) technique (on compressing barriers) alpha phase can be converted to beta phase [50]. PVDF exhibits a piezoelectric property in beta phase which is useful for sensor applications [51]. It expands or contracts based upon the direction of applied electric field. It can store electric charge when pressure is applied [51]. Ferroelectrics such as PVDF can be used as tunnel barriers in Metal/Ferroelectric/Metal junctions since they exhibit dynamic switching of dielectric polarization on application of an electric field [52],[53]. PVDF along with copolymer trifluoroethylene which forms P(VDF-TrFE) is considered to be the best actuator [49]. PVDF exhibits potential properties in ferroelectric and piezoelectric thin film devices compared to its copolymer P(VDF-TrFE) [54]. PVDF is used as a binder for making electrode materials [55]. When taken in 10:1 ratio of activated carbon (AC):PVDF, it shows better capacitance when compared to only AC [19]. It can be used along with NMP solvent as a binder to make slurry like mixture

[56],[55],[57]. Study shows that, with increase in dielectric constant, there is improvement in energy density. To increase the energy storage in the electrochemical capacitors, highly polarizable nanocomposites are used [58]. The improved dielectric constant of the composite material results in very high energy density [58]. We see that, on solution mixing and further processing with other materials like graphite nanoplatelets, PVDF enhances the dielectric constant and electrical conductivity of the formed nanocomposite [59].

Energy density in the dielectric material is directly proportional to the product of the dielectric constant and the square of the electrostatic field present [58]. Moreover, dielectrics are very useful in acting as tunnel barriers and could avoid the self leakage effect seen in supercapacitors. All these properties are an added advantage to the PVDF material used as dielectric layer for supercapacitor applications. G-PANI nanocomposite exhibits very high surface area and very high specific capacitance [37],[36]. The surface area of the material may be improved by coating the G-PANI with a material exhibiting polarizable nature such as PVDF with high dielectric constant. The polarization of the PVDF is achieved by alignment of permanent dipoles and this can be done by horizontal deposition using the LB [50]. The mechanism and the mode of deposition are covered in detail in the next section. The change of material lattice resulting in change of alpha phase to beta phase can be achieved without any poling treatment using the LB technique [50]. The ferroelectric polymer PVDF (C-C) main chains are arranged parallel to the subphase and the dipole moment is perpendicular to the subphase surface [50]. Since PVDF is not completely amphiphilic in nature, they are arranged differently from what we see in normal Langmuir film where the hydrophobic end is towards air and the

hydrophilic part is towards water. The C-F groups of PVDF molecule form hydrogen bonds with O-H groups of water molecule. The C-F groups are arranged towards the water and the C-H groups are away from the water. Hence we see the C-C main chains are parallel to the water surface [60]. Figure (12) depicts the schematic sketch of the proposed alignment.

(a)   *(b)*
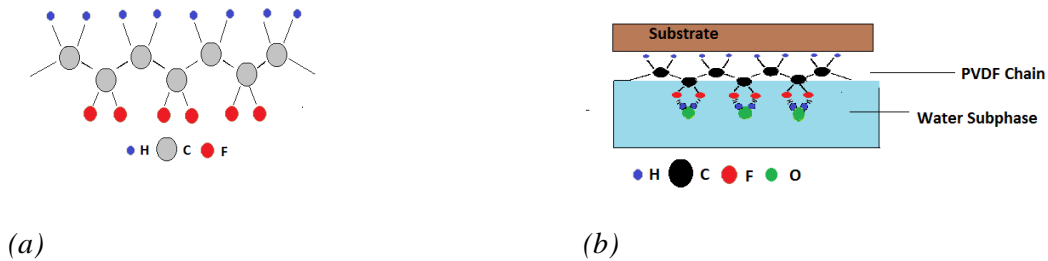
Figure 12: (a) Beta phase on water subphase, (b) Schematic sketch of alignment of PVDF on substrate

The following chapters give detailed study on specific capacitance with and without the presence of PVDF monolayer. A self leakage experiment is conducted to understand the leakage effect on the electrode material with the presence of monolayer/monolayers of PVDF.
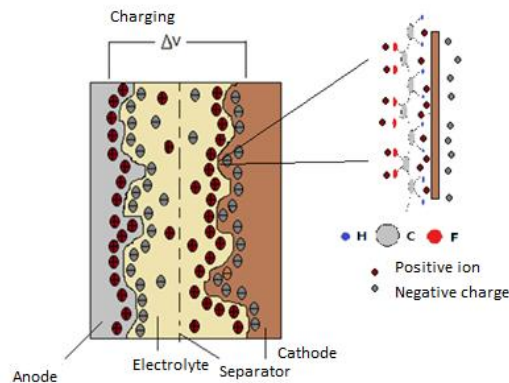
Figure 13: Schematic sketch of PVDF chain on G-PANI substrate as electrode material

2.3 Langmuir Blodgett (LB) /Langmuir-Schaefer (LS) Techniques

PVDF monolayer is deposited using the LB technique. This is very useful in changing the phase of PVDF from alpha to beta [50],[60]. LB technique is one of the most promising technologies to deposit very thin and uniform molecular level monolayers of different organic materials [61]. It gives very precise control over the monolayer thickness and state of phase [62]. It is used to deposit very homogeneous monolayer over large surface area. Multilayer films can be prepared. Structures with two different surfactants of different orientation or layer composition can be defined. Large varieties of surfactants can be deposited over different substrates [63]. Exploitation of organic materials in electronic and optoelectronic devices at the molecular level can be done using LB technique [61]. Surfactants are a huge class of molecules which are amphiphilic in nature having hydrophobic (water hating) and hydrophilic (water loving) parts. This amphiphilic nature is due to the formation of micelles, bilayers, vesicles, etc. When surfactant comes in contact with any solution such as water, the physical and chemical properties of the surfactants affect the association behavior and their affinity for interface with the solution. Surfactant needs to be insoluble in water. It can be spread onto the trough carrying subphase with help of any volatile and water insoluble solvent as shown in figure (14).
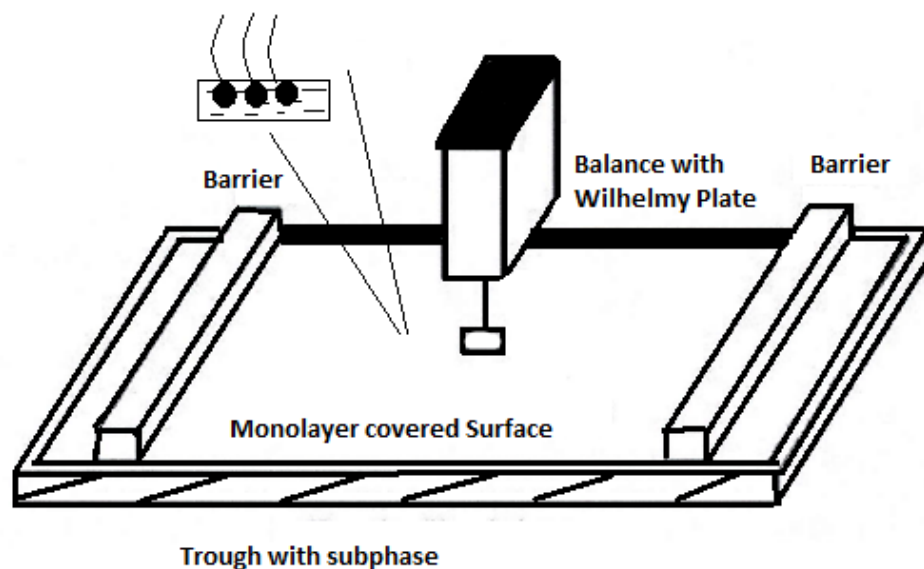
Figure 14: LB trough carrying subphase

When surfactant comes in contact with water, it accumulates at the interface causing a decrease in surface tension of water [61]. The dielectric constant of water at 20° C is 80.1. Dielectric constant can measure the solvent's ability to reduce the field strength of the electric field surrounding a charged particle immersed in it. Polar compounds mix with only polar solvents whereas non-polar compounds mix with non-polar solvents. Surface tension is the measure of energy per unit area. The interface possesses some free energy due to the difference in the environment of the molecules at the surface and inside the water. This free energy can be defined using the surface tension. Surface tension of water is 73 mN/m at 20 ^{o}C. Any material spread over water cannot exhibit surface pressure more than this value. Surface pressure is the difference between the surface tension without the surfactant molecules and surface tension with the molecules spread onto the subphase. Surface tension can be measured with the help of Wilhelmy balance shown in

figure (15). The software program directly gives the value of surface pressure. A Wilhelmy plate is very thin, and is generally made of platinum, quartz or a filter paper. Paper plates are generally used as Wilhelmy balance for LB measurement since they become saturated with water, both the receding and the advancing contact angles will become zero. The mean molecular area can be calculated by monitoring over the distance covered by the barriers in the trough of known dimensions. Isotherm taken is the surface pressure measured with respect to the mean molecular area. The figure (16) shows different phase states on compression of barriers. This is due to increase in surface pressure. Initially, the molecules are in gaseous state, and then liquid–gaseous state, then liquid state, and finally solid state [64]. Further compression would lead to collapse of the film. At this solid phase, film can be easily transferred onto the substrate. At this point, there is high cohesion maintained in the molecules resulting in smooth transfer without falling apart. Hence a constant surface pressure is maintained during deposition.
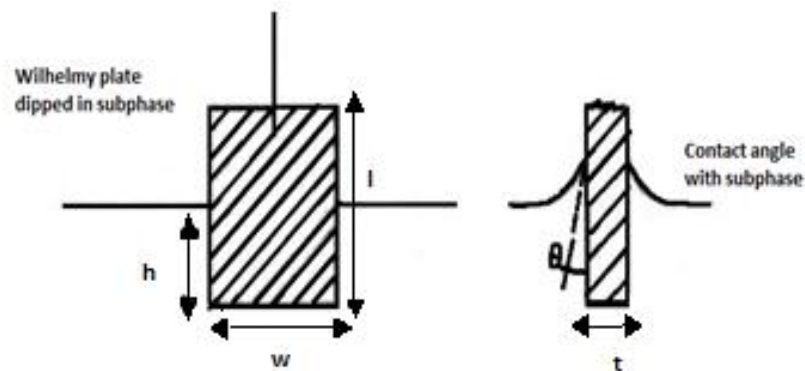
Figure 15: Wilhelmy plate in subphase.
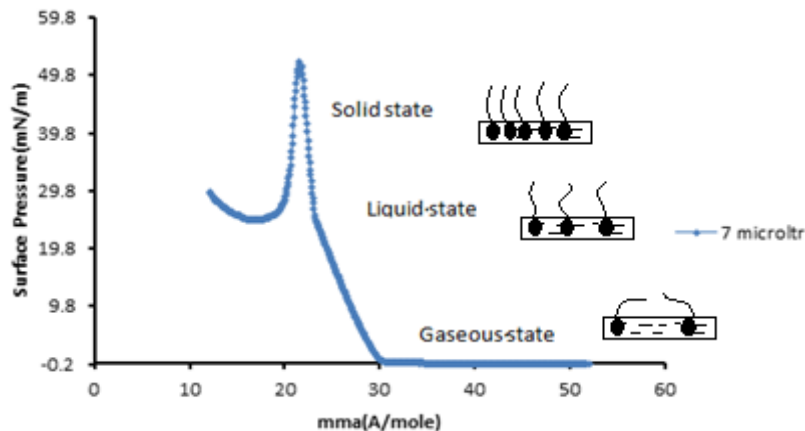
Figure 16: Stearic acid isotherm

Stearic acid isotherm is generated using 1 mg/ml concentration solution of chloroform solvent to understand the phase state transition on compression of barriers. Different phase states are shown in the figure (16). 25 mN/m is the appropriate surface pressure at which the film can be deposited onto the substrate. On compression of barriers, phase state transition takes place from gaseous state to liquid state and from liquid state to solid state. For stearic acid isotherm, the mean molecular area (mma) is observed above 30 Å/mole in gaseous state and mma from 20 to 30 Å/mole represents the liquid state. Below mma 20 Å/mole is the solid state. Deposition of the film onto any substrate is done at this point in order to have smooth and complete transfer of the film. Above this point, the film breaks. Any material surface can be hydrophobic or hydrophilic based upon the surface chemistry and surface roughness. Materials of low energy are considered to be hydrophobic and materials of high energy are hydrophilic in nature.

Figure 17: Water droplet on hydrophobic and hydrophilic surface

Water droplets on hydrophobic and hydrophilic substrate depict the nature of the surface. Contact angle (θ) defines the nature of the surface of any material. If θ>90°, surface is hydrophobic else hydrophilic. If θ>150°, surface is superhydrophobic and if θ<5°, it is superhydrophilic in nature. Two types of depositions are possible with LB, which are vertical deposition and horizontal deposition. Films based on vertical deposition are called LB films whereas on horizontal deposition are called LS films. The film formed on the subphase surface on compression of barriers is called Langmuir film.
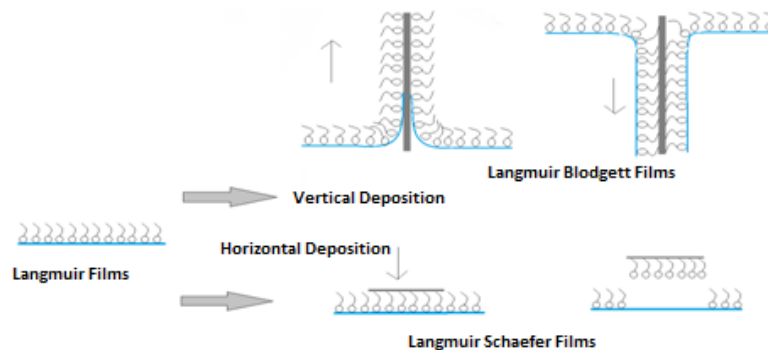
Figure 18: Types of deposition using LB

Transfer Ratio (TR) is the ratio of the area decrease on the sub-phase surface to the area covered by the dipped substrate. It is the measurement for efficiency in vertical deposition technique. Value ranges from 0 to 1, where 1 indicates perfect deposition. Three different types of configurations with LB deposition are possible. X type configuration is where depositions occur only on down strokes for a substrate which is

hydrophobic in nature. Z type configuration is where depositions occur only on up strokes for a substrate which is hydrophilic in nature. Y type configuration is where depositions occur on up stroke and then down stroke, repeatedly for a substrate which is hydrophilic in nature. Langmuir Schaefer film depositions are done by horizontally dipping the substrate onto the subphase surface. If the substrate is hydrophobic, X type configuration is possible. If the substrate is hydrophilic, Z type configuration is possible.
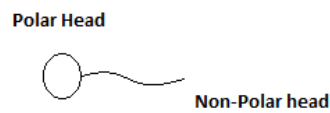
Figure 19: Amphiphilic molecule
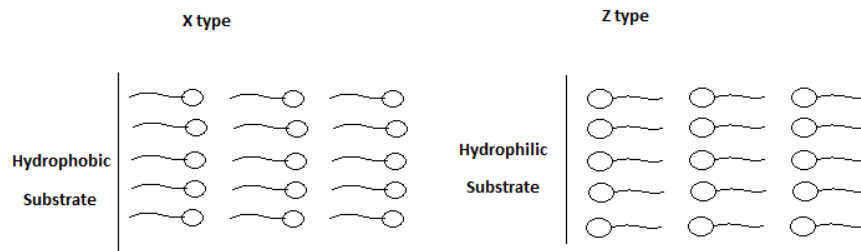
Figure 20: X and Z type configurations
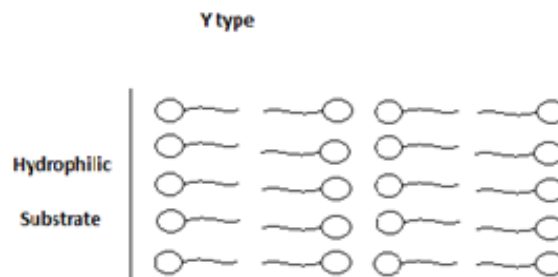
Figure 21: Y type configuration

Vertical deposition for hydrophilic substrates is done by immersion of substrate beforehand in subphase water and then isotherm is generated. Optimum surface pressure is maintained for deposition. Dipping starts on programming the setup. Odd number of layers can be deposited. Vertical deposition for hydrophobic substrates is done by hanging the substrate in the air with the hold of dipper. Isotherm is generated and deposition is done at optimum surface pressure. In this case, even number of layers can be deposited.

CHAPTER 3: EXPERIMENTAL SETUP

3.1 List of Materials used for Experiments

Aniline ($\geq$99.5%), ammonium persulfate ($\geq$98%), sodium hydroxide ($\geq$97%) and hydrochloric acid (37%) were all purchased from Sigma–Aldrich (USA) and were ACS graded. N-N-dimethylformamide (99.8%) and 1-methyl-2-pyrrolidinone (99.5%) were also purchased from Sigma-Aldrich in anhydrous form. Poly (vinylidene fluoride) (pellets) with dielectric constant (8-9.5) was also purchased from Sigma-Aldrich. Pristine graphene powder (platelets with thickness ranging from 50-100nm) was purchased from Angstrom Materials (USA). The materials and chemicals were procured from commercial companies which were used without further purification unless and until it is specified.

3.2 Langmuir Films of PVDF

PVDF platelets were dissolved in dimethylformamide (DMF) solvent using sonication for speed dissolution [50]. The concentration of the PVDF-DMF solution was taken to be 1 mg/ml. The Langmuir isotherm of PVDF was studied by spreading different amount of solution on Langmuir trough at constant temperature. The solvent (DMF) was made to evaporate by spreading known quantity of PVDF solution on trough for 30 minutes. Programming was done to compress the barriers and to get an isotherm of the PVDF. The compressed monolayer PVDF film on top of the water subphase is called the Langmuir

film. Suitable surface pressure for deposition is known from different isotherms generated by taking different volumes of the mixed solution (PVDF-DMF) using KN2001 small LB deposition trough from KSV NIMA Group. The perfect isotherm is established using 50 µl of solution and the optimum surface pressure for deposition is selected as 25 mN/m. The surface pressure of the monolayer steeply decreased upon reaching 25 mN/m which indicates a condensed state of the film. Hence surface pressure of 25 mN/m is chosen for deposition.
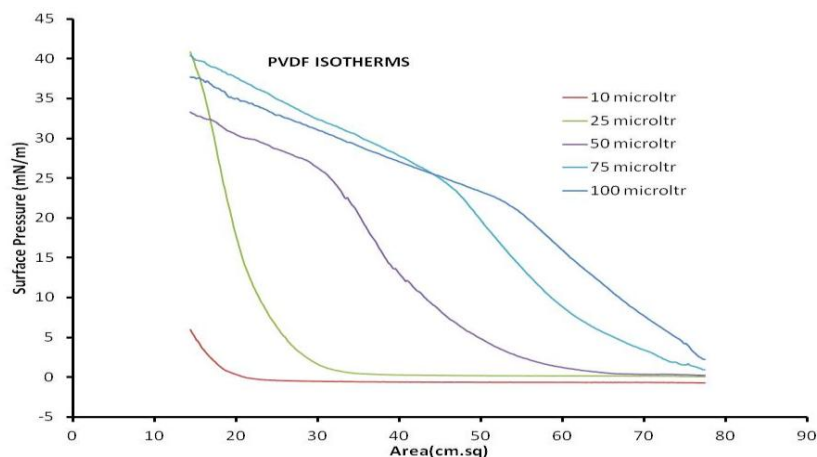
Figure 22: PVDF isotherms as a function of amount of material distributed at air/water subphase
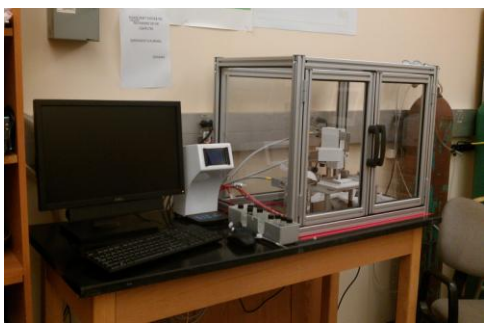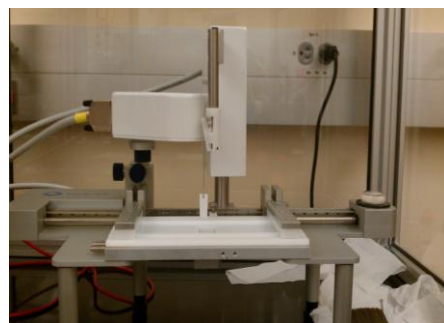
(a)   (b)

Figure 23: (a) LB instrument in lab, (b) Trough carrying water subphase

35

3.3 Synthesis of Graphene-Polyaniline Nanocomposite

Chemical oxidative polymerization technique is used to synthesize the G-PANI nanocomposite [37]. It is synthesized by oxidative polymerization of 0.2M aniline with 0.05M ammonium persulfate $(NH_4)_2S_2O_8$ in 1M HCl. Graphene to aniline weight is taken in the ratio of 1:2. Ammonium persulfate solution is added slowly drop by drop to the aniline and graphene mixture maintained in an ice bath at 4 ^{o}C under constant stirring. It is then stirred for 24 hrs continuously and it is kept still for 8-10 hours for the entire polymerized material to settle down. It is then filtered and washed with DI water, ethanol and methanol to remove any unwanted low molecular weight polymers and oligomers. The recovered material is then heated at 100 ^{o}C constant temperature in an oven for about 8 hrs and then cooled down to room temperature 50^0C for about 12 hrs. The yield obtained is 7.026 g out of 13.965 g. The obtained is in doped form. To make it un-doped, it is immersed in 1M sodium hydroxide (NaOH) for 24 hrs. It is then filtered, washed and dried as mentioned above. The material can be drop-casted on to any substrate like silicon, ITO, glass, graphite, etc. using solvent 1-methyl-2-pyrrolidinone (NMP). It basically acts as a plasticizer to get a very smooth film of G-PANI nanocomposite.
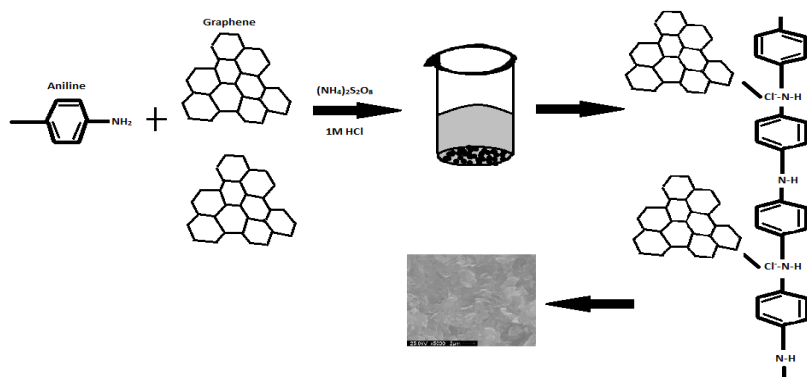
Figure 24: Schematic sketch of G-PANI synthesis [37]

3.4 Electrochemical Cell Setup

Electrochemical cell setup consists of three electrodes with sample for testing as the work electrode, platinum mesh as the counter electrode and Ag/AgCl as the reference electrode with 1 M HCl as the electrolyte, unless specified a different concentration of electrolyte.
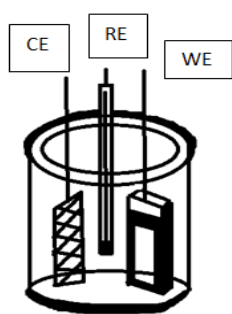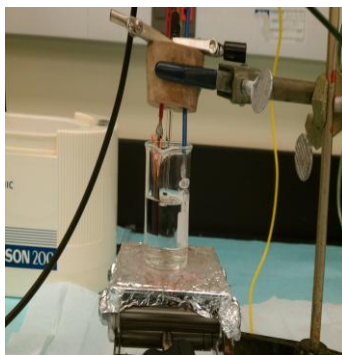
| (a) | (b) | (c) |

Figure 25: (a) Schematic sketch of a cell setup, (b) Laboratory cell setup, (c) Active surface area defined on sample

3.5 Sample Preparation

Desired sample is prepared and it is then coated with a stop off lacquer to define the active surface area to be dipped inside the electrolyte solution. This ensures the correct calculation of surface area in contact with the electrolyte. All electrochemical measurements are done using Volta lab 40 analyzer from Radiometer Analytical Company.
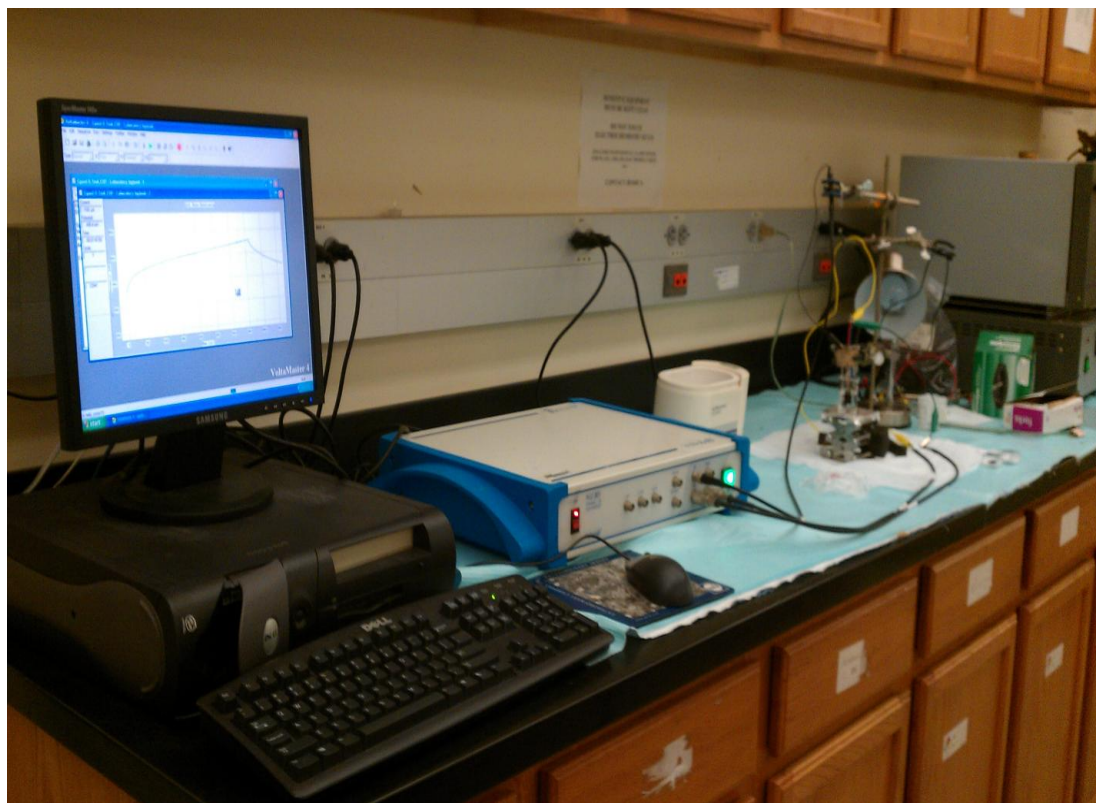
Figure 26: Voltalab analyzer in lab

CHAPTER 4: ELECTROCHEMICAL INVESTIGATION

4.1 Graphene Polyaniline Nanocomposite (G-PANI)

Graphite is chosen as the substrate for the electrode material. It is cleaned thoroughly using ethanol, methanol and DI water. It is then dried at 100 ^{o}C to evaporate the absorbed solvents. It is then weighed to get the desired weight of the graphite. G-PANI is a nanocomposite material which can be drop casted onto the substrate with the help of N-Methyl-2-pyrrolidone (NMP) solvent. It is then dried at 100 ^{o}C to make sure that the entire NMP solvent is evaporated. It is then weighed again to get the desired amount of G-PANI material present on the substrate. It is then doped with 1M HCl. A thin film is deposited onto the substrate.
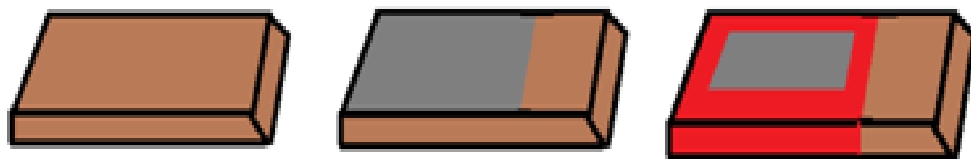
Figure 27: Schematic sketch of the sample-G-PANI

The area of the sample used is 1.23 cm^2 and the mass was found to be 1.07 mg. The cyclic voltammetry (CV), electrochemical impedance spectroscopy (EIS) and charge-

discharge experiments are done in 1M HCl electrolyte in a three electrode system configuration.
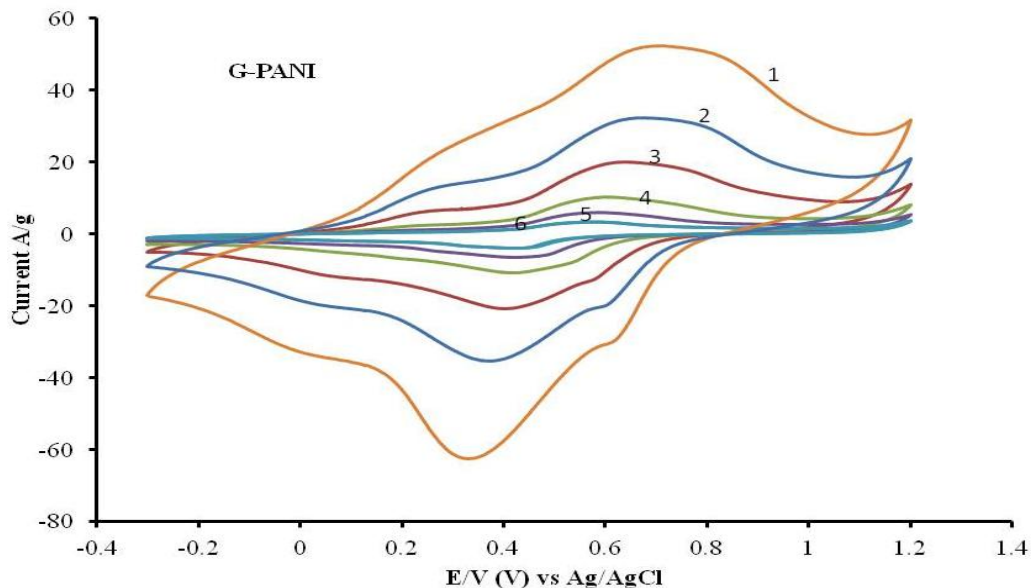
Figure 28: Cyclic voltammetry of G-PANI at different scan rates 1) 200 mV/sec, 2) 100 mV/sec, 3) 50 mV/sec, 4) 20 mV/sec, 5) 10 mV/sec and 6) 5 mV/sec

Cyclic voltammetry is a useful technique to understand the capacitive behavior of the electrode material. This is done by cycling a repetitive linear potential sweep across the two fixed and defined voltages. The current flowing through the electrochemical cell is measured with respect to potential. A constant sweep potential rate (scan rate) is used to calculate the flow of current. The experiment is conducted at different scan rates. Lower scan rates take longer time for testing compared to time taken for higher scan rates.

We see the cyclic voltammetry of G-PANI exhibiting a pseudocapacitive behavior involving charge transfer mechanism which is due to the incorporation of the polyaniline conducting polymer in the nanocomposite material. Interestingly, in addition, graphene

also exhibits the electrochemical behavior in the aqueous and organic electrolytes [37]. G-PANI under diffusion controlled system sustaining reversible redox processes contributes both electric double layer capacitance and pseudocapacitance, indeed increasing the overall capacitance of the electrode material. The voltage limits are from -0.3V to 1.2V, optimum enough to avoid electrolyte decomposition and breakdown of electrode material consequently. The NMP solvent acts as a very good binder for graphene-polyaniline nanocomposite material. The specific capacitance values calculated at different scan rates 200 mV/sec, 100 mV/sec, 50 mV/sec, 20 mV/sec, 10 mV/sec and 5 mV/sec are listed below. The CV response of all scan rates is observed to follow a certain trend; time dependent current values changes with the change in scan rate, depicting the behavior of an electrochemical material completely reversible in nature as shown in figure (28). It has been observed that a decrease in scan rate is related to the increase of specific capacitance, likely due to getting more time for ions to diffuse through the nanopores of the electrode material in electrochemical reactions. The film deposited is very thin; hence the specific capacitance values are higher in number comparatively. We observe that the specific capacitance values increase with decrease in scan rate depicting the complete usage of the electrode material during the electrochemical redox processes. G-PANI exhibits oxidation and reduction peaks which are attributed to the different forms of polyaniline. Estimation of capacitance from figure (28) is found using the formula $C = I_p/v_s$, where I_p is the peak current and v_s is the scan rate.

Table 5: G-PANI: The specific capacitance vs. scan rate

Scan rate (mV/sec)	200	100	50	20	10	5
G-PANI (F/g)	284.57	338	406	519.25	610.5	713
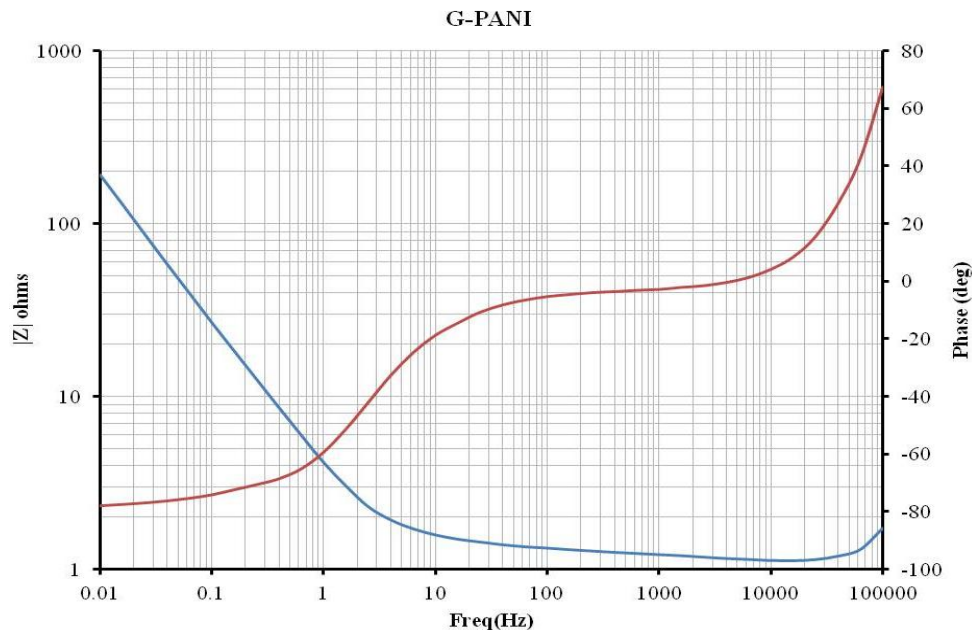
Figure 29: Bode plot of G-PANI

Electrochemical impedance spectroscopy is a useful technique to study the material properties under time dependent current conditions, measuring the overall impedance |Z| as a function of frequency and related to overall capacitance of the electrochemical cell. It proves to be very useful in capacitive behavior analysis. The measurement is done again in the three electrode system configuration with 1M HCl with Ag/AgCl reference and platinum mesh electrodes at open circuit potential. It is measured over 100 kHz to 10 mHz frequency range. The corresponding impedance values |Z| (ohms) and phase (deg) are plotted versus each frequency value. The figure (29) depicts the Bode plot, showing capacitive behavior of the G-PANI electrode material. It is very useful in measuring the series resistance (R_s), apparent capacitance corresponding to each frequency and leakage resistance (R_l). Internal resistance is evaluated from bode plot at higher frequency (10 kHz) and capacitive behavior at low frequency (0.01 Hz).The inductive effect at 100 kHz

42

is due to usage of long enough wires that act as inductors. Using the Software, the parameters are determined to be R_s=1.42 ohms, C=0.04 F, R_l=53.53 ohms.
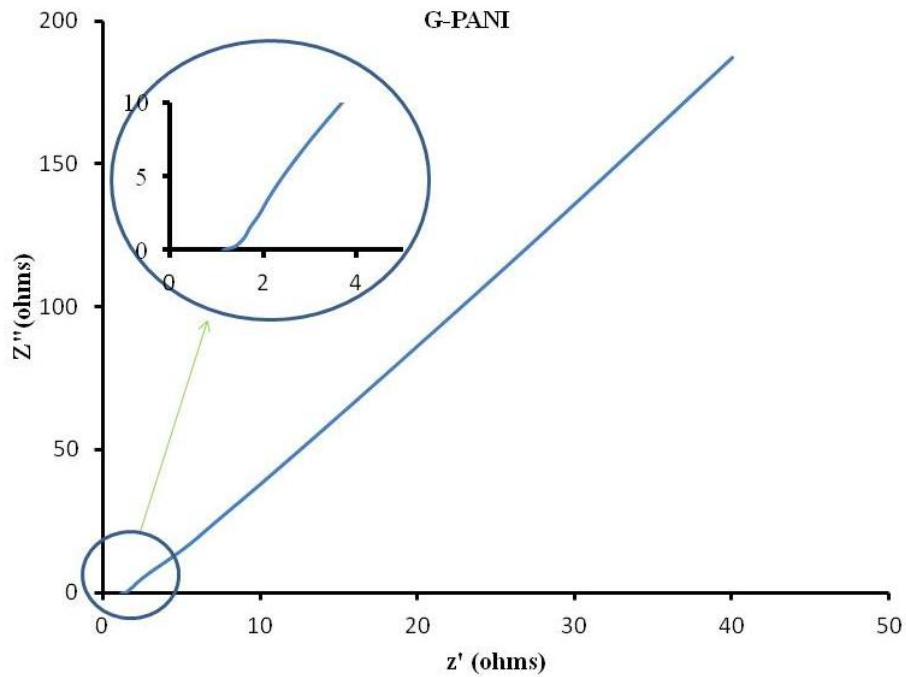
Figure 30: Nyquist plot of G-PANI

Nyquist plot is another form of representing EIS data. The Nyquist plot in figure (30) depicts the excellent capacitive behavior of the G-PANI nanocomposite. The behavior at very high frequency depicts the diffusion controlled system. The R_s is very small in the order of few ohms (1-1.5) suggesting much less internal series resistance, which is depending on conductivity or molar concentration of the electrolyte used. The low impedance values indicate the highly capacitive nature of the G-PANI electrode material.
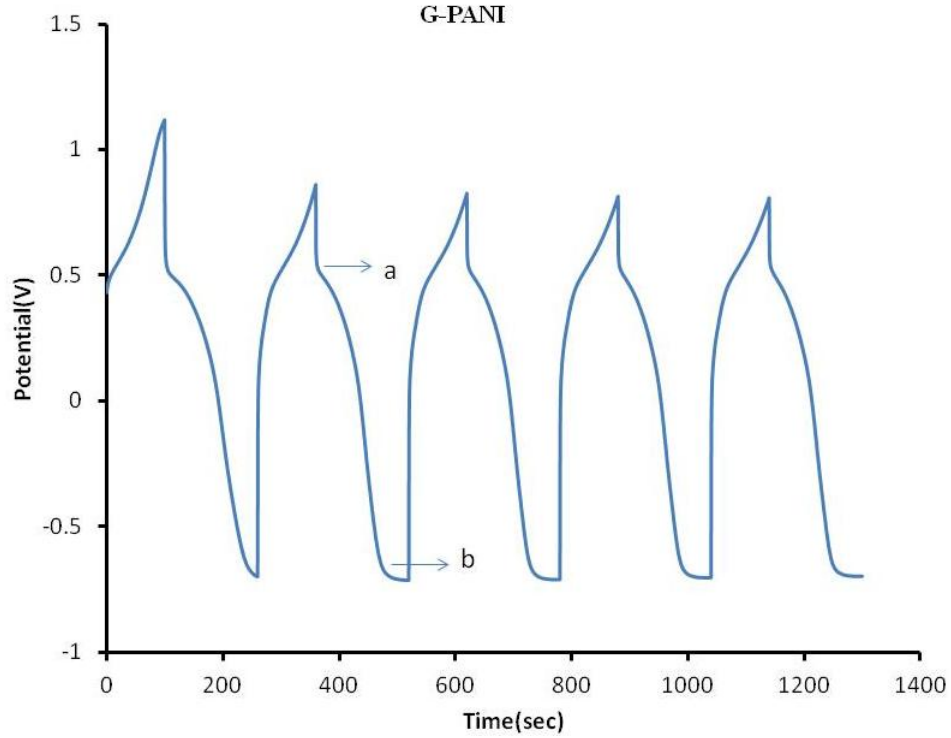
Figure 31: Charge-discharge curves for G-PANI at 1-mA charging and discharging currents

Charge-discharge tests are conducted using chronopotentiometry technique as a part of electrochemical characterization. This technique is based on charging the electrode material by applying constant current and measuring the potential difference linearly with respect to time across the cell.

A higher series resistance results in large IR drop, which reduces the power density of the supercapacitor. The specific discharge capacitance based on the discharge profile is determined to be 81.1 F/g from voltage difference between (a) and (b) in figure (31).The capacitor is charged at 1 mA for 100 sec and discharged completely for 160 sec. The charging and discharging times are much less, adding additional advantage to the

44

electrode material enhancing capacitor performance. The energy density and power density can be evaluated with charge discharge curves. They become useful parameters in capacitor performance as an energy storage device.

4.2 PVDF Film on Graphite (PVDF)

Clean graphite is taken as the substrate. PVDF Langmuir film is prepared as mentioned previously with the use of LB Instrument. Horizontal dipping of the substrate onto the water subphase is done to obtain LS film of PVDF monolayer.
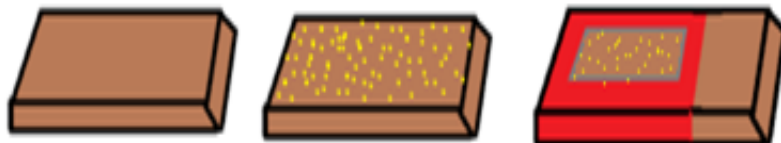
Figure 32: Schematic sketch of the PVDF film on graphite

Areas of the graphite substrate with PVDF monolayer and of graphite are taken to be 1 cm^2. CV and EIS measurements are done to study the capacitive behavior of the PVDF monolayer and to compare the results with plain graphite. This study will be very useful in analyzing the capacitive behavior of PVDF, since it is a ferroelectric polymer. The CV measurement proved to be very useful in understanding the electrochemical nature of the PVDF. The curves at different scan rates follow a trend of decrease of time dependent current with respect to different scan rates as shown in figure (33). The peak current is directly proportional to the square root of the scan rate. This clearly shows it is exhibiting electrochemical behavior suggesting it is an electroactive material undergoing reversible electrochemical reactions. The monolayer PVDF is exhibiting high peak redox currents

which are shown in the CV curve. This material is exhibiting very interesting electrochemical behavior in diffusion controlled system with charge transfer phenomena in play. The CV clearly shows the electrode material is completely reversible in aqueous electrolyte. The voltage range is taken from -0.3V to 1.2V, which is used as the optimum potential limits for G-PANI. The PVDF monolayer as an electrode material is effectively working without any breakdown in this voltage window. So this material can be used along with G-PANI efficiently. The oxidation peak and reduction peaks are at 0.97V and 0.6V with a peak current of 4 mA at 5 mV/sec scan rate. Interestingly, at 200 mV/sec scan rate, two oxidation and reduction states are observed. Moreover due to the dipole alignment of the PVDF molecules in beta phase, there is a possibility to increase the surface area, increasing the specific capacitance of the electrode material. The C-F molecules are dipole arranged towards the electrolyte, resulting in high surface area. A very interesting behavior is observed here, the change in current density with respect to scan rate is much less.
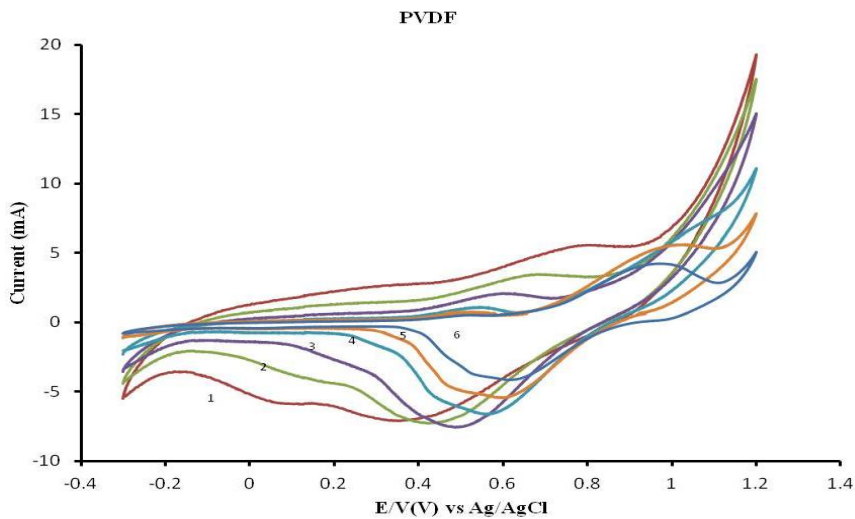
Figure 33: Cyclic voltammetry of PVDF at different scan rates 1) 200 mV/sec, 2) 100 mV/sec, 3) 50 mV/sec, 4) 20 mV/sec, 5) 10 mV/sec and 6) 5 mV/sec
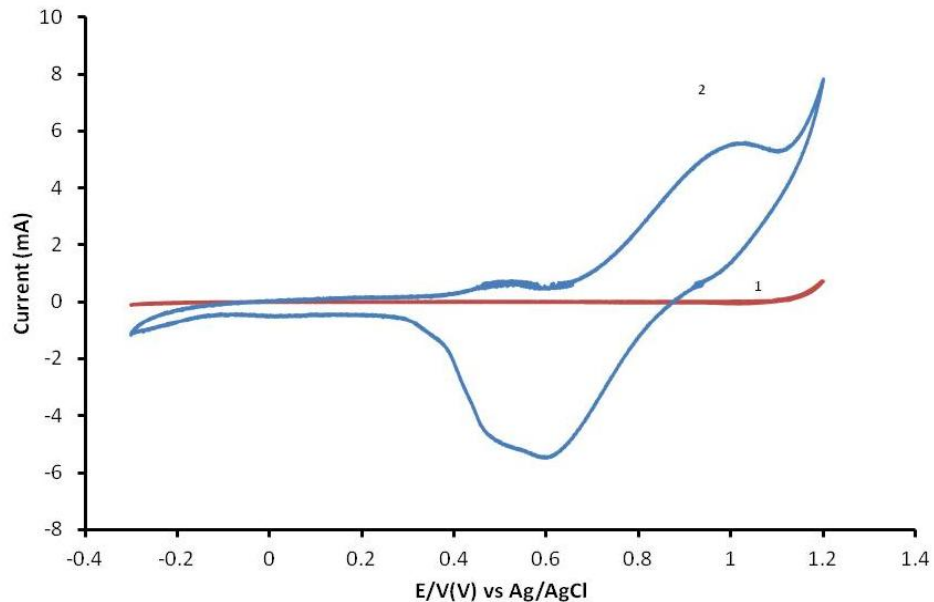
Figure 34: Cyclic voltammetry at 10 mV/sec scan rate for 1) Graphite and 2) PVDF

The figure (34) represents comparing the CV curves for PVDF versus graphite at 10 mV/sec scan rate. This depicts the complete redox system of PVDF under diffusion controlled environment. The charge transfer mechanism undergoing suggests PVDF to be an electrochemical material. The reversible redox system with oxidation peak at 1V and reduction peak at 0.6V respectively at 10 mV/sec scan rate is observed in the CV. It shows a wider and larger potential window in comparison to only graphite substrate which clearly proves high specific capacitance resulting with the use of PVDF very aligned molecular dipole monolayer.

47
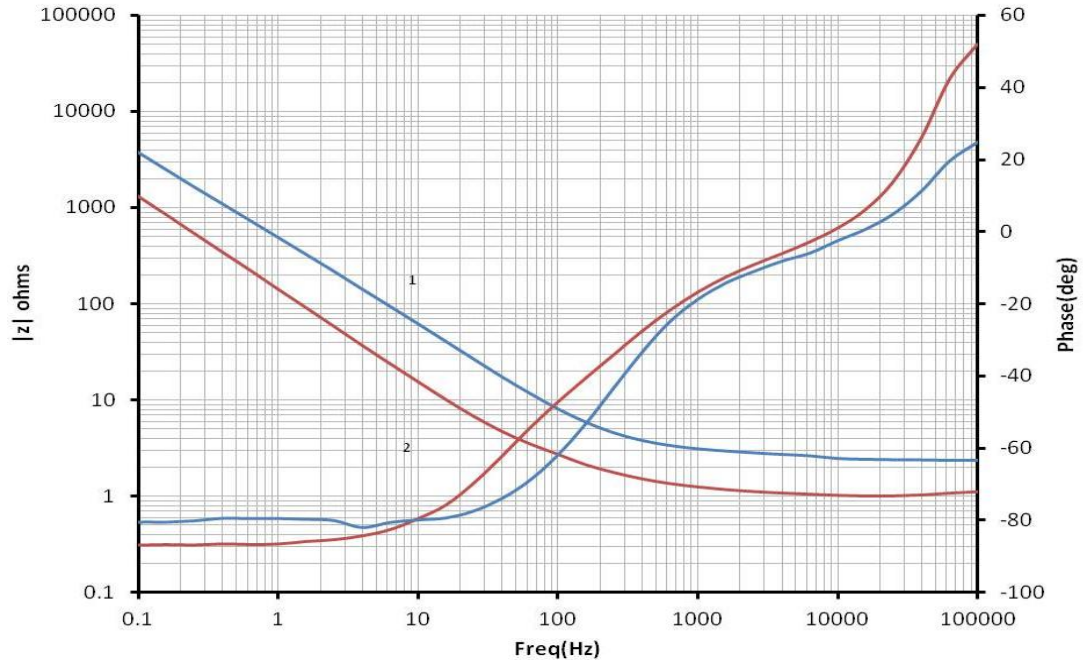
Figure 35: Bode plot for 1) Graphite and 2) PVDF

The Bode plot is made using the data from EIS study. The measurement is done in 100 kHz to 0.01 Hz frequency range and the corresponding |z| and phase values are plotted here. From the above Bode plot in figure (35), it clearly indicates the capacitive behavior of PVDF with respect to graphite. For instance, the impedance value at 1 Hz for PVDF is less compared to the impedance value for graphite, suggesting higher capacitance of PVDF due to the inverse relation between the apparent capacitance with the impedance value at that frequency. The plot show highly conducting and capacitive PVDF monolayer, hence we do not expect lower leakage current.
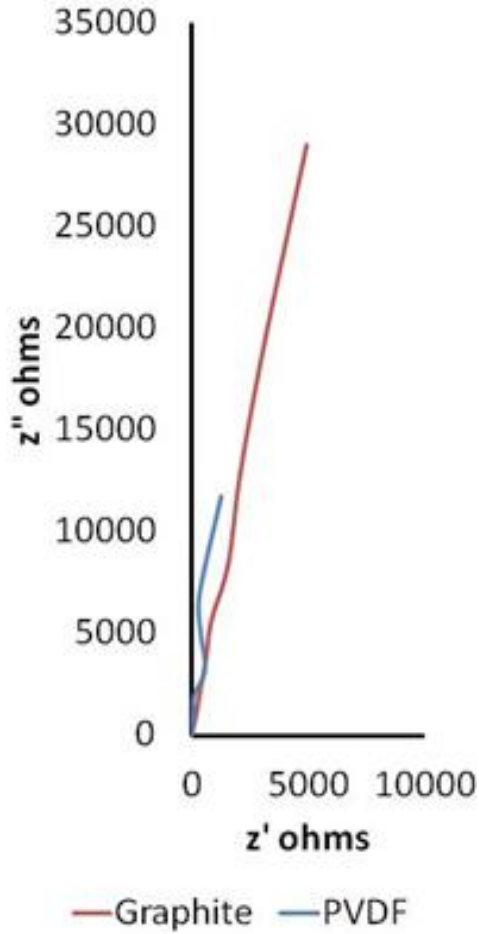
Figure 36: Nyquist plot for graphite and PVDF

Nyquist plot proved to be an excellent parametric design to understand the behavior of PVDF. The plot in figure (36) clearly indicates the increase in capacitance with the presence of PVDF layer on a graphite substrate. The graphite is said to show high impedance value, depicting a lower capacitive nature, whereas PVDF is exhibiting lower impedance values resulting in a higher capacitance. This proves that, PVDF is an excellent material to be used for enhancing the supercapacitor performance in terms of capacitance, but not better for reducing the leakage current.

The data in 1 Hz to 100 kHz frequency range is analyzed using software to get the parameters of Randle's circuit, to better understand the supercapacitor electrochemical cell.

Table 6: Randle's model parameters for graphite and PVDF on graphite

Sample	R_s ohms	C_{dl}	R_l ohms
Graphite	2.79	240.5 uF	1363
PVDF	1.289	936.4 uF	759.8

On application of PVDF, we see that the double layer capacitance was increased, which might be due to the increase in surface area because of much aligned and dipole structure of PVDF on graphite and due to the electrochemical nature of the material. The model will help us to understand the impedance behavior of the supercapacitor. The series resistance is also observed to be very small limiting the power loss, there by contributing to the high power density.

4.3 Graphene- Polyaniline Nanocomposite with PVDF as Prime Layer

Clean graphite is taken as substrate for electrode. PVDF monolayer is deposited by horizontal deposition using Langmuir Blodgett technique to obtain a Langmuir Schaefer film. The G-PANI nanocomposite is drop casted on top of the monolayer using NMP solvent. It is then dried at 100 ^{o}C. The PVDF layer is said to be the prime layer to G-PANI.
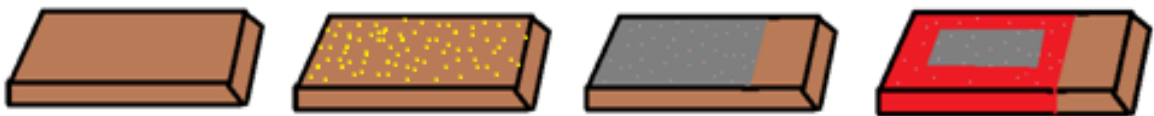
Figure 37: Schematic sketch of the G-PANI with PVDF as the prime layer

The apparent area of the substrate was defined to be 1.65 cm^2 and mass found to be 1.65 mg. Electrochemical measurements such as CV, EIS and charge-discharge tests are conducted to analyze the capacitive behavior on applying PVDF monolayer as a prime layer to the G-PANI nanocomposite. The CV curves are obtained for different scan rates. The voltage limits are kept from -0.3V to 1.2V, suitable and optimum potential limits for G-PANI and same cell configuration is used for comparison purposes. We observe a very nice CV profile as shown in figure (38), depicting the same as G-PANI nanocomposite with the oxidation and reduction peaks. This suggests that the peaks are due to the different forms of polyaniline existing due to the incorporation of PANI conducting polymer in the nanocomposite. We also observe a nice flow of trend between all the scan rates, stating the electrode material to be electrochemically active in nature. We also observe that the specific current at a certain scan rate 10 mV/sec is almost same as that of G-PANI as shown in figure (50). Suggesting the use of PVDF as prime layer did not prove to be of much use as an enhancement to the capacitance of the electrode material. The area of the voltage window gives the intuition of the surface area and hence the specific capacitance of the electrode material. The area of the window seems to be same as in the case of G-PANI. This might be due to the very nice and smooth NMP based G-PANI film, which is not allowing the PVDF to be in contact with the electrolyte to exhibit its property. However, the use of PVDF as prime layer did not degrade the performance of the G-PANI nanocomposite. We observe the wide voltage window here depicting the specific capacitance is almost same as that of the G-PANI electrode.
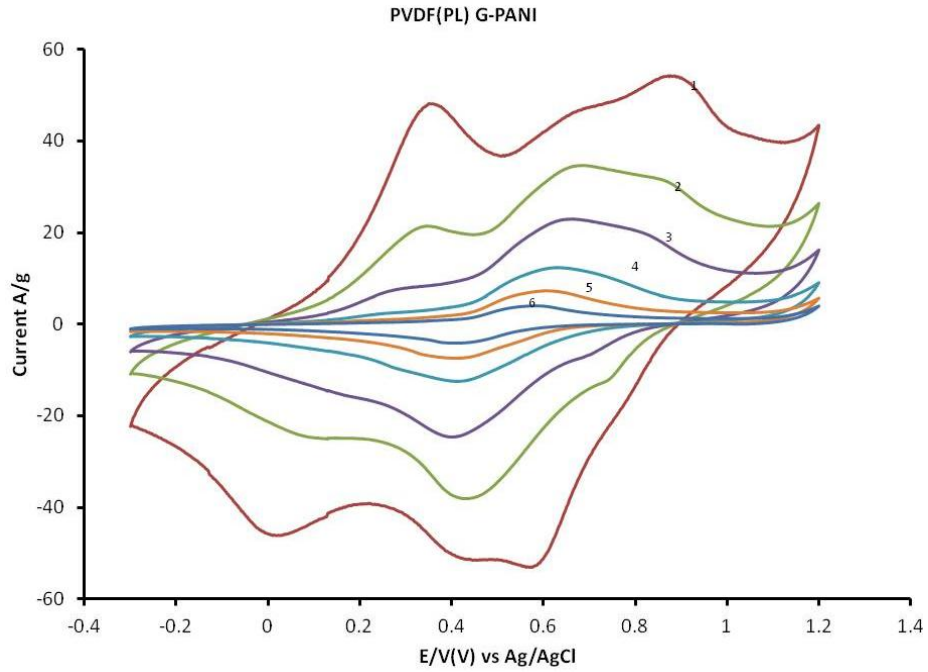
Figure 38: Cyclic voltammetry of PVDF (PL) G-PANI at different scan rates 1) 200 mV/sec, 2) 100 mV/sec, 3) 50 mV/sec, 4) 20 mV/sec, 5) 10 mV/sec and 6) 5 mV/sec
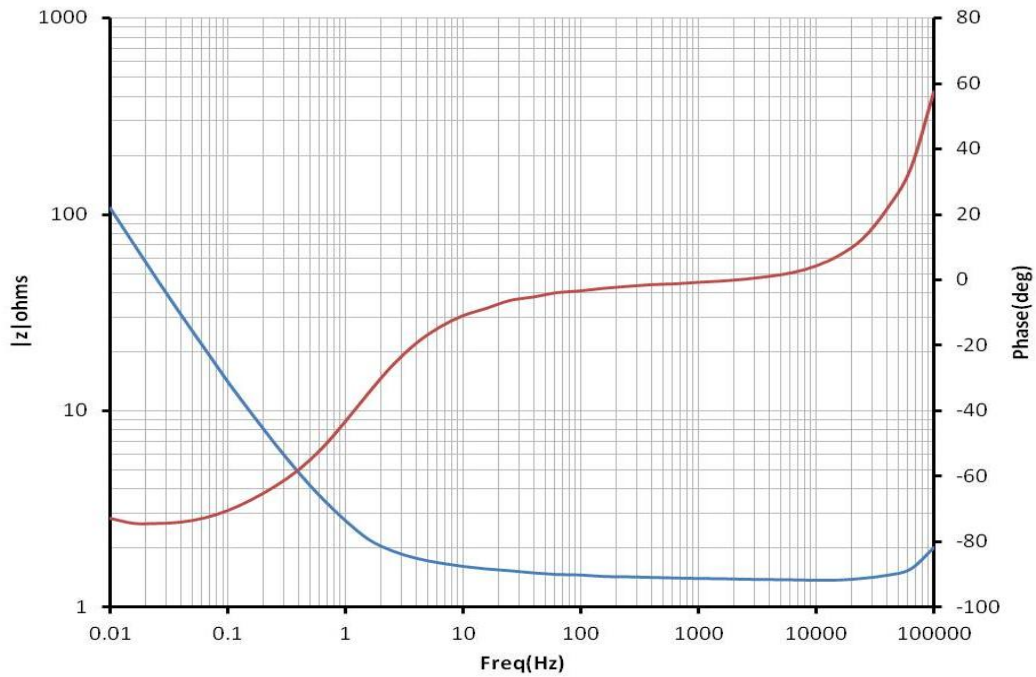
Figure 39: Bode plot of PVDF (PL) G-PANI

Bode plot and Nyquist plot depict the capacitive nature of the electrode material. Useful data regarding the series resistance, overall capacitance and leakage resistance can be interpreted. PVDF acts as a very good binder to the G-PANI electrode. The Nyquist plot depicts diffusion controlled system.
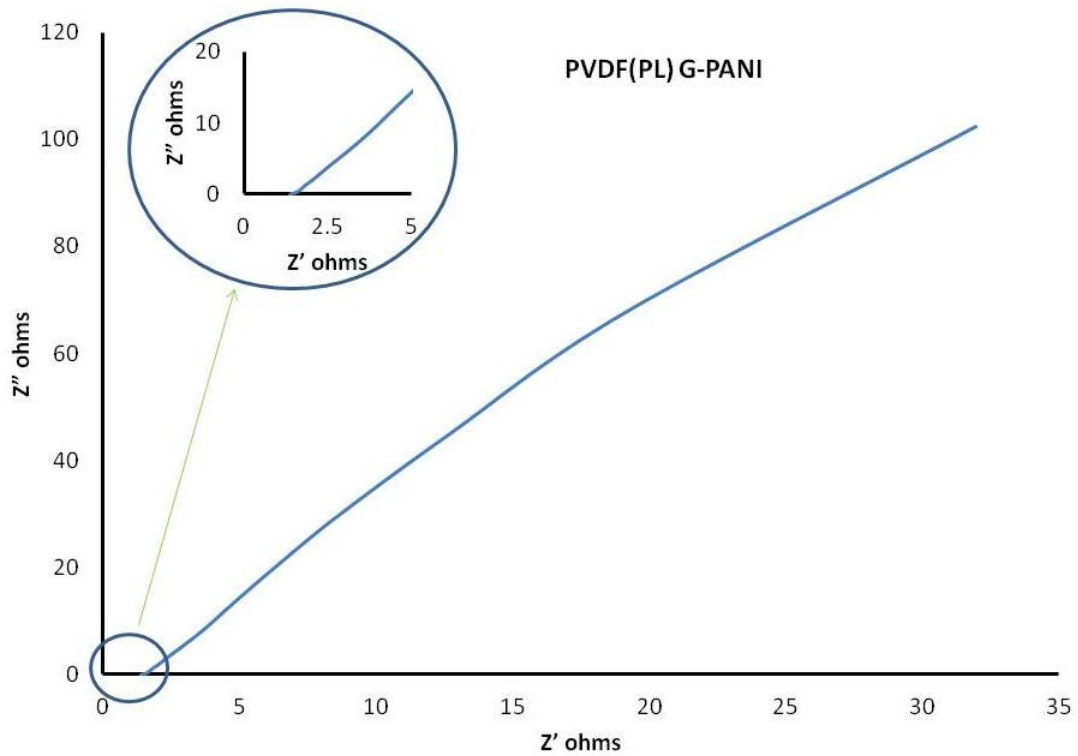
Figure 40: Nyquist plot of PVDF (PL) G-PANI

4.4 Graphene- Polyaniline Nanocomposite – PVDF Monolayer

Clean graphite is taken as the electrode substrate. A thin film of graphene-polyaniline nanocomposite (G-PANI) is drop casted using NMP. It is then coated with PVDF monolayer Langmuir Schaefer film by horizontal deposition using Langmuir Blodgett technique to get G-PANI PVDF.
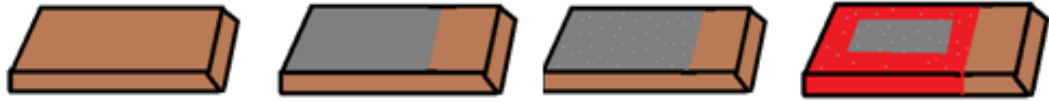
Figure 41: Schematic sketch of the G-PANI PVDF

Area defined on the substrate to be 1.65 cm^2 and mass found to be 1.11 mg on loading the

substrate with the electrode material.
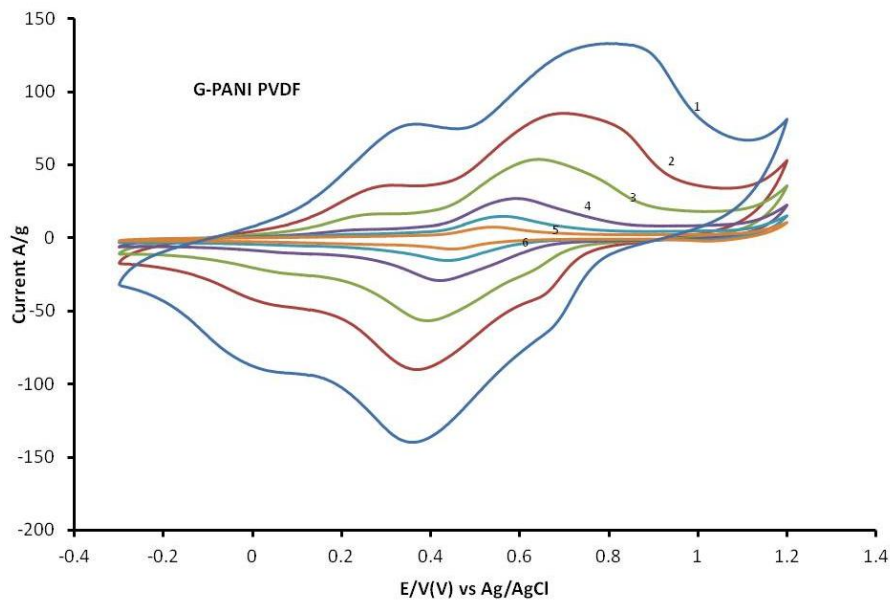
Figure 42: Cyclic voltammetry of G-PANI PVDF at different scan rates 1) 200 mV/sec,
2) 100 mV/sec, 3) 50 mV/sec, 4) 20 mV/sec, 5) 10 mV/sec and 6) 5 mV/sec

Cyclic voltammetry tests are run on the sample at different scan rates to identify the

specific capacitance corresponding to each scan rate. The voltage limits are -0.3V and

1.2V, the perfect voltage window to avoid electrolyte decomposition and breakdown of

electrode material. Interestingly, the application of PVDF on G-PANI shows an increase

in specific capacitance than G-PANI based supercapacitor. It was calculated to be almost

54

doubled at each and every scan rate. The profile of the CV curve in figure (42) depicts the pseudocapacitive nature of the electrode material involving redox mechanisms undergoing charge transfer reactions. The peak currents are proportional to the square root of the scan rate. This effect explains the reversible electron transfer reactions undergoing in diffusion controlled system. PVDF is an electroactive chemical in nature sustaining faradic reactions, at the same time due to the dipole alignment of PVDF molecules, there is a possibility to have high surface area electrode material enhancing specific capacitance. The wider potential window depicts an increase in specific capacitance of the material compared to G-PANI. Interestingly, the CV curve here can also be used to interpret the unknown states existing in between the fully reduced leucoemeraldine state, emeraldine salt and base, between the fully oxidized pernigraniline states due to the incorporation of very thin monolayer of PVDF. The CV characteristics might depict some information on careful analysis and interpretation.

Table 7: G-PANI PVDF: The specific capacitance vs. scan rate

Scan rate (mV/sec)	200	100	50	20	10	5
G-PANI PVDF (F/g)	679.55	876.25	1098.3	1384.25	1480	1506
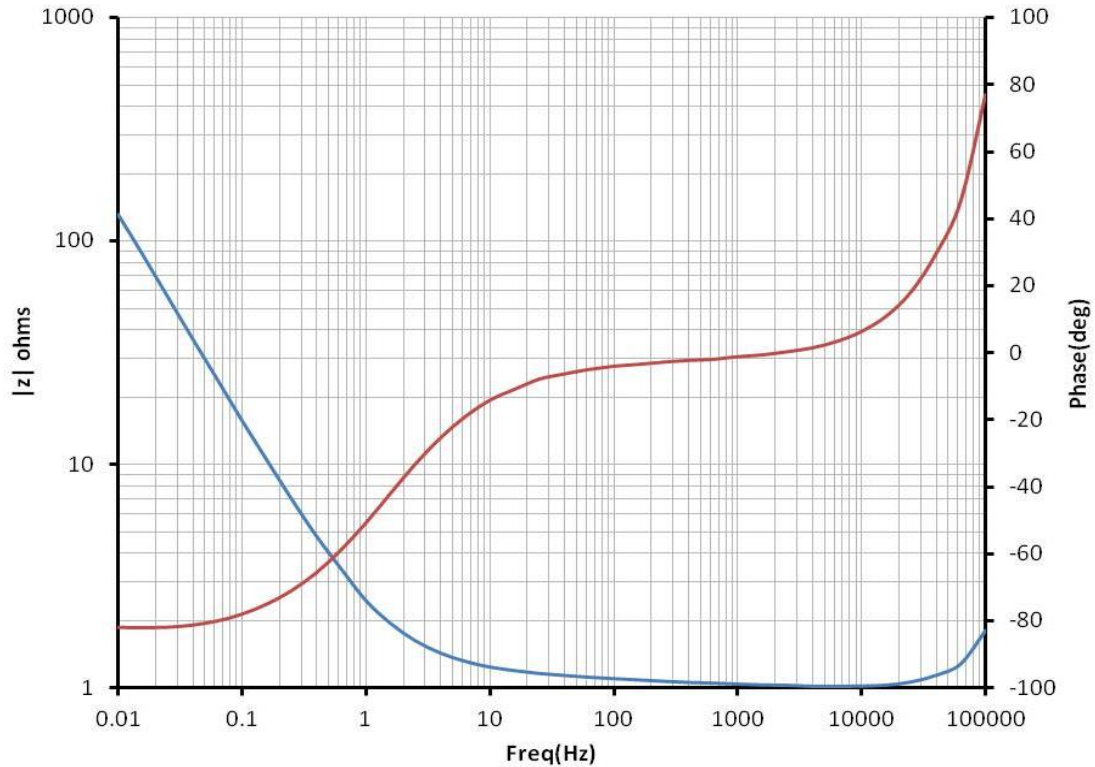
Figure 43: Bode plot of G-PANI PVDF

The EIS study is done at open circuit potential in the three electrode cell configuration gives valuable information regarding the ESR, capacitive effect and leakage resistance. The semi circle at high frequency in the Nyquist plot depicts the diffusion controlled system. The G-PANI PVDF electrode material is said to be more capacitive in nature qualitatively with respect to G-PANI, which is proved with the EIS study. The main advantage of such measurement is time dependent response. It saves the electrode material from damage due to high currents used as in case of CV and charge-discharge measurements. The EIS study proved that with the application of dielectric thin film PVDF aligned monolayer, the capacitance is increased greatly contributing to the electrode performance.
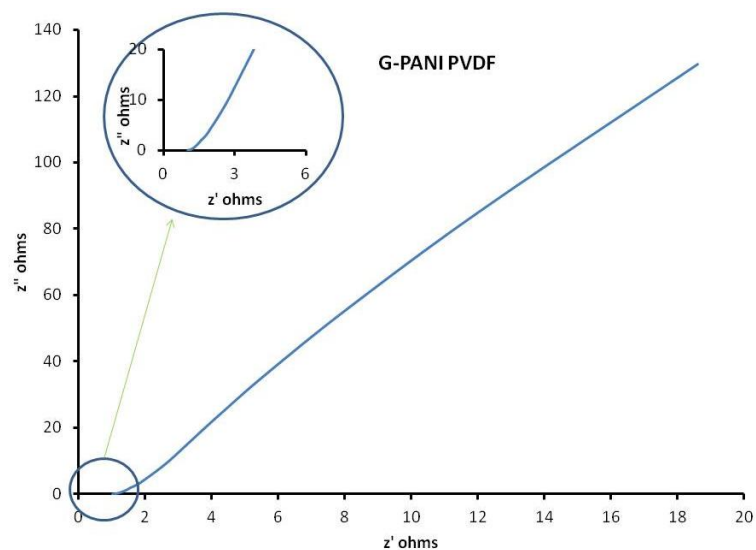
Figure 44: Nyquist plot of G-PANI PVDF
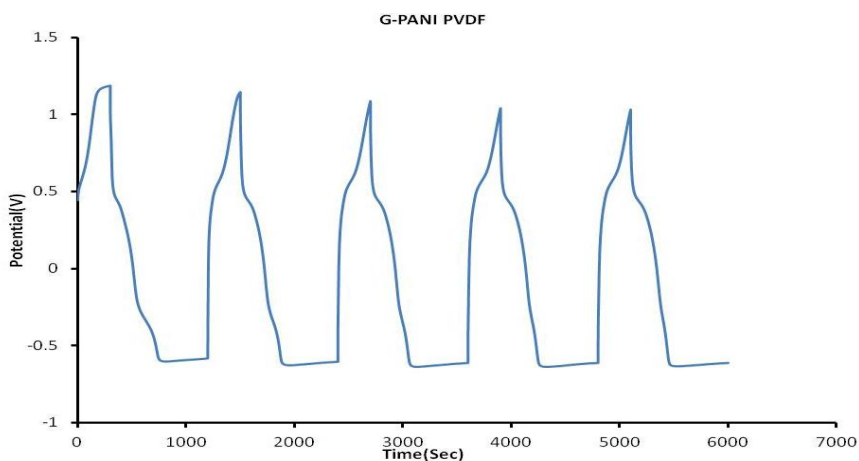
Figure 45: Charge discharge curves for G-PANI PVDF at 1 mA charging and discharging currents

The electrode material G-PANI with PVDF monolayer is charged with a charging current of 1 mA for about 5 min to attain a rated voltage of about 1 V and made to discharge with discharging current of 1 mA for 15 min to attain 0V. The time taken to charge and

discharge is more relatively compared to the time taken for G-PANI. This clearly proves the increase in energy density for the electrode material where PVDF is incorporated. The specific discharging capacitance of 248.94 F/g is observed at 1 mA specific current. This value is quite impressive in comparison to the G-PANI specific discharging capacitance which is 81.8 F/g.

4.5 Comparison Study between G-PANI and G-PANI PVDF

It is highly important to analyze the capacitive behavior of G-PANI, both with and without the presence of PVDF monolayer. The thin molecular size PVDF dipole aligned monolayer on the G-PANI substrate is making a lot of difference in specific capacitance values and is responsible for storing high energy per unit time, increasing the energy density of the electrode material. The CV, EIS study and charge-discharge tests are conducted to study the nature of these electrodes. All the measurements helped in understanding the change in behavior of the systems.
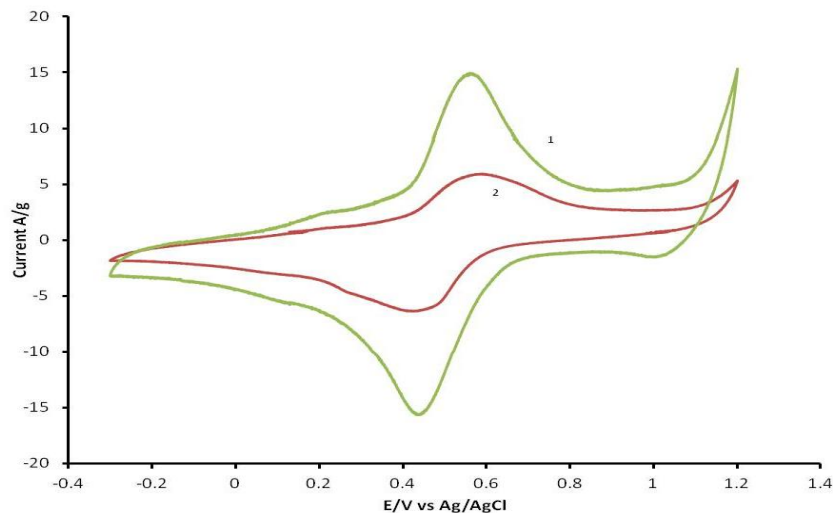
Figure 46: Cyclic voltammetry of 1) G-PANI PVDF and 2) G-PANI at 10 mV/sec scan rate

We can observe that the specific capacitance is higher for G-PANI PVDF when compared to only G-PANI as shown in figure (46). A molecular monolayer of PVDF is responsible for high increase in surface area and also due to its electrochemically active nature results in an increase in specific capacitance value.

The CV measurement gives the identity of the faradic reactions, in both G-PANI and G-PANI PVDF. Due to the undergoing redox mechanisms, as expected the CV curve exhibited the deviations in the profile. The potential window limits depend on the nature of the electrode material. For comparison purposes, the limits are taken as same in both the cases i.e. -0.3V to 1.2V. We observe that PVDF material on graphite can work efficiently without breaking down in this potential window. Electrolyte molar concentration is responsible for any deviations in the profile. Hence 1M HCl is used to compare results. The CV clearly shows the effect of pseudocapacitance which is due to polyaniline-conducting polymer and graphene incorporation; moreover as from previous results, we also observe that PVDF is electrochemical in nature exhibiting the reversible electrochemical reaction. Hence G-PANI PVDF exhibits the same behavior with increase in redox peak currents comparatively. The CV profile shows a larger voltage window depicting higher surface area and higher specific capacitance for G-PANI PVDF. Moreover the oxidation and reduction states which are due to different forms of polyaniline i.e. leucoemeraldine fully reduced form, emeraldine base and salt and fully oxidized form of pernigraniline states are visible in both the G-PANI and G-PANI PVDF.

Figure 47: Charge discharge curves for 1) G-PANI PVDF and 2) G-PANI at 1 mA charging and discharging currents

Area of the substrate is defined as 1.23 cm^2 and mass found to be 1.07 mg for G-PANI electrode, whereas area of 1.65 cm^2 and mass of 1.11 mg is defined for G-PANI PVDF. G-PANI reached a rated voltage of 1.1V within 100 sec and time taken to discharge through 0V is 150 sec, whereas G-PANI PVDF reached a rated voltage of 1V with 5min and time taken to discharge through 0V is 15 min as shown in figure (47). This indicates the high energy storage in G-PANI PVDF.

The specific discharge capacitance obtained for G-PANI at 1 mA current density is 81.1 F/g and where as for G-PANI PVDF is 248.94 F/g. The area under the charging and discharging curve indirectly depicts the surface area, hence the associated specific capacitance and specific energy density can be known. It is quite evident from the figure (47) the discharge time taken for G-PANI PVDF to reach 0V from the maximum rated voltage is more, indicating increase in specific energy density. This might be due to the

increase in surface area due to the dipole alignment of the PVDF molecules on the G-PANI. The electrochemical nature of PVDF is another added advantage to the effectiveness of the electrode material G-PANI.
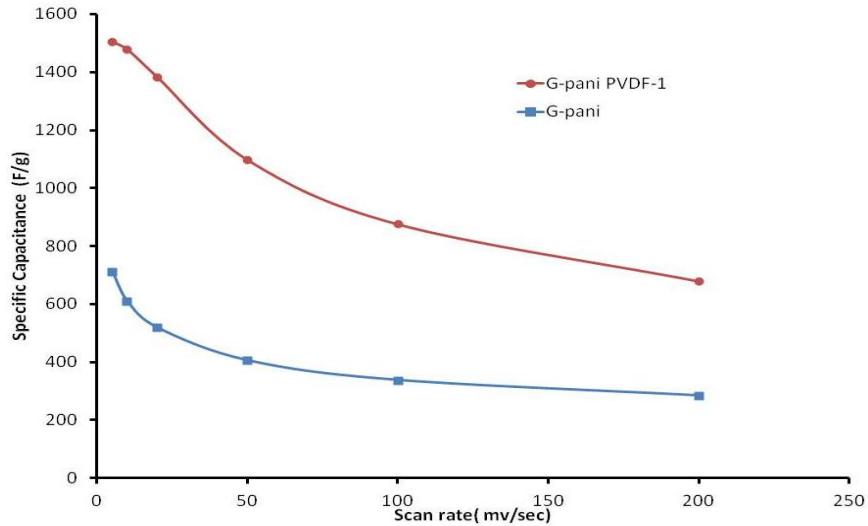
Figure 48: Comparison of specific capacitance for G-PANI and G-PANI PVDF at different scan rates

Table 8: Comparison of specific capacitance for G-PANI & G-PANI PVDF

Scan rate (mV/sec)	200	100	50	20	10	5
G-PANI (F/g)	284.57	338	406	519.25	610.5	713
G-PANI PVDF (F/g)	679.55	876.25	1098.3	1384.25	1480	1506

The figure (48) and table (8) depicts the comparison of specific capacitance values obtained from cyclic voltammetry for G-PANI and G-PANI PVDF. High specific capacitance values are obtained with the presence of PVDF monolayer on G-PANI nanocomposite.
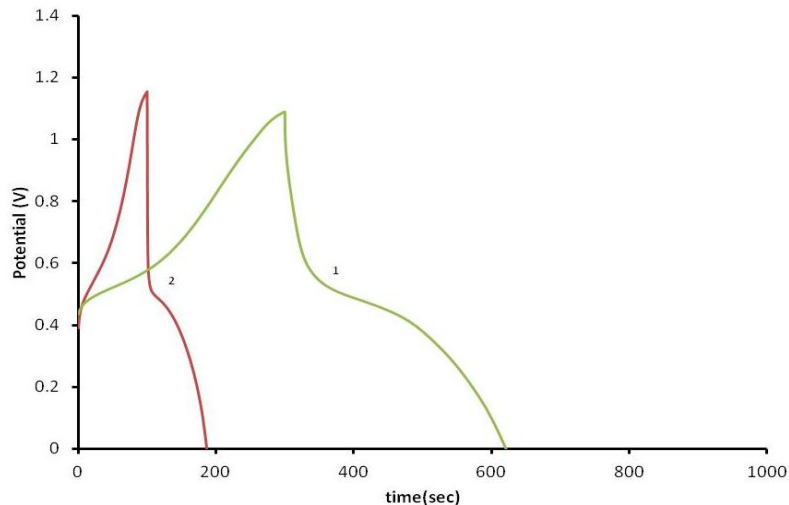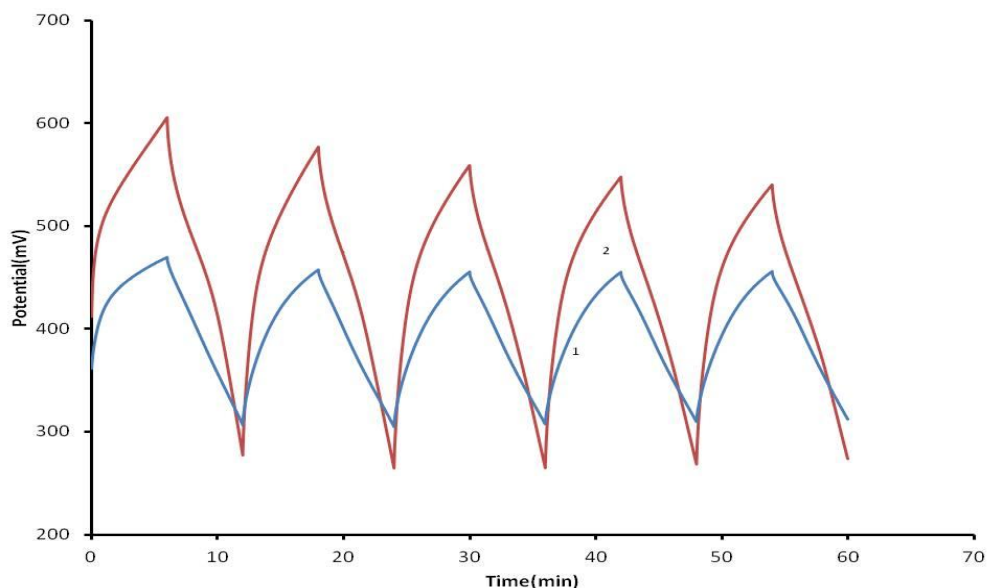
Figure 49: Charge discharge curves for 1) G-PANI PVDF and 2) G-PANI at 0.1mA charging and discharging currents

Area of the substrate is defined as 1.17 cm^2 and mass of 0.94 mg for the G- PANI electrode, whereas area of 1.7 cm^2 and mass of 1.5 mg for the G-PANI PVDF electrode. The charging and discharging profile at 1 mA for both G-PANI and G-PANI PVDF shows a very nice capacitive nature of the electrode materials. For comparison purposes, the charging time and discharging times of 6 min each is kept constant for both the types. As shown in figure (49), the G-PANI achieved higher voltage compared to G-PANI PVDF suggesting G-PANI PVDF has the higher energy storage capability; hence a higher specific capacitance is associated with G-PANI PVDF which is the same as observed in the discharge profile.

Below are results obtained from processing the EIS files using ZsimDemo 3.20 version software (ZsimpWin) from Princeton Applied Research [65].

Table 9: Randle's circuit model parameters for G-PANI and G-PANI PVDF

Sample	Rs ohms	C_{dl}(F)	R_l ohms
G-PANI	1.42	0.04458	53.32
G-PANI PVDF	1.282	0.08474	45.2

The frequency range from 0.1 Hz to 100 kHz is considered for analysis of impedance behavior for the supercapacitor. The solution resistance is almost the same in both the cases, in the range of 1-1.5 ohms. The double layer capacitance was increased on application of PVDF dipole aligned monolayer which might be due to enhancement in surface area due to the much aligned molecular structure of PVDF.

Table 10: Randle's circuit model with constant phase element parameters for G-PANI and G-PANI PVDF

Sample	Rs(ohm)	C_{dl}(F)	R_l (ohms)	Q	n	R(ohms)
G-PANI	1.401	0.038	1163	0.0288	0.8844	21.51
G-PANI PVDF	1.261	0.066	2246	0.03752	0.8784	6.708

The frequency range from 0.01 Hz to 100 kHz is considered for impedance behavior analysis of the supercapacitor. Using the constant phase element model, it is seen that the value of n is around 0.8, suggesting nearly ideal double layer capacitance. We also see the double layer capacitance increased on application of PVDF monolayer on G-PANI nanocomposite. It is almost double the capacitance of G-PANI.

4.6 Comparison Study between G-PANI, PVDF (PL) G-PANI, GPANI PVDF
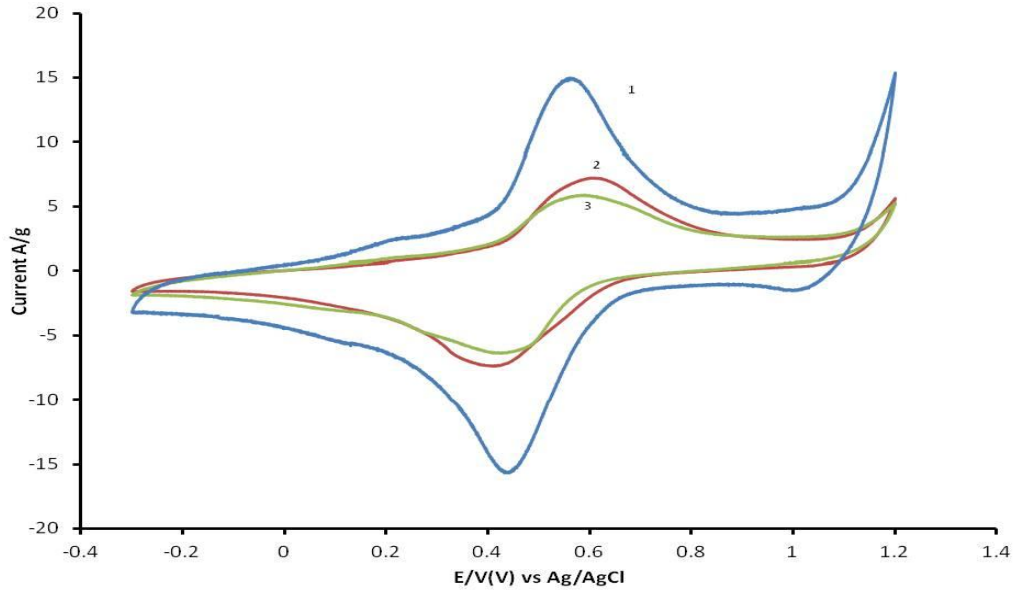
Figure 50: CV of 1) G-PANI PVDF, 2) PVDF (PL) G-PANI and 3) G-PANI at 10 mV/sec rate

From the figure (50) of cyclic voltammetry, we see that PVDF (PL) G-PANI is having the same specific capacitance as that of G-PANI. This might be due to very smooth layer of NMP (acting as a plasticizer) casted G-PANI, which is not allowing the PVDF monolayer to have electrolyte contact and hence there is no enhancement in specific capacitance. PVDF on G-PANI nanocomposite shows significant increase in area of the voltage window, depicting higher surface area and specific capacitance.

4.7 Graphene-Polyaniline Nanocomposite –2 Layers of PVDF Coating

G-PANI nanocomposite is drop casted onto the substrate, and then 2 layers of PVDF is deposited using horizontal deposition technique to have Langmuir Schaefer films. Area

64

of the substrate is defined as 1.7 cm^2 and mass found to be 0.9 mg for G-PANI PVDF2 electrode. CV tests are conducted in aqueous medium of 1M HCl using the three electrode cell maintaining the same conditions. Potential sweeps are done at different scan rates from -0.3V to 1.2V, which is the optimum range to avoid electrolyte decomposition. The CV profile in figure (51) shows deviations due to the pseudocapacitive effect of both graphene and polyaniline (PANI) conducting polymer and due to the presence of very thin monolayers of PVDF, an electrochemical active material which is showing redox properties. 2 layers of PVDF on G-PANI contributed to the overall specific capacitance due to its participation in faradic redox reactions at the electrode/electrolyte interface under diffusion controlled environment. The CV area depends upon the electrochemical reactions and surface area of the electrode material. Redox peak currents are proportional to the square root of scan rate, indicating that reversible electrochemical reactions took place, suggesting electrode material is electrochemically reversible in nature. The oxidation and reduction peaks observed which are due to the highly reversible conducting polymer –polyaniline existing in different forms. We see that the specific capacitance is not as high as the G-PANI PVDF; this might be due to the presence of second layer of PVDF which is hindering the surface area covered in the G-PANI PVDF. It is studied to see the effect on specific capacitance and in the latter section to understand the behavior of self leakage.
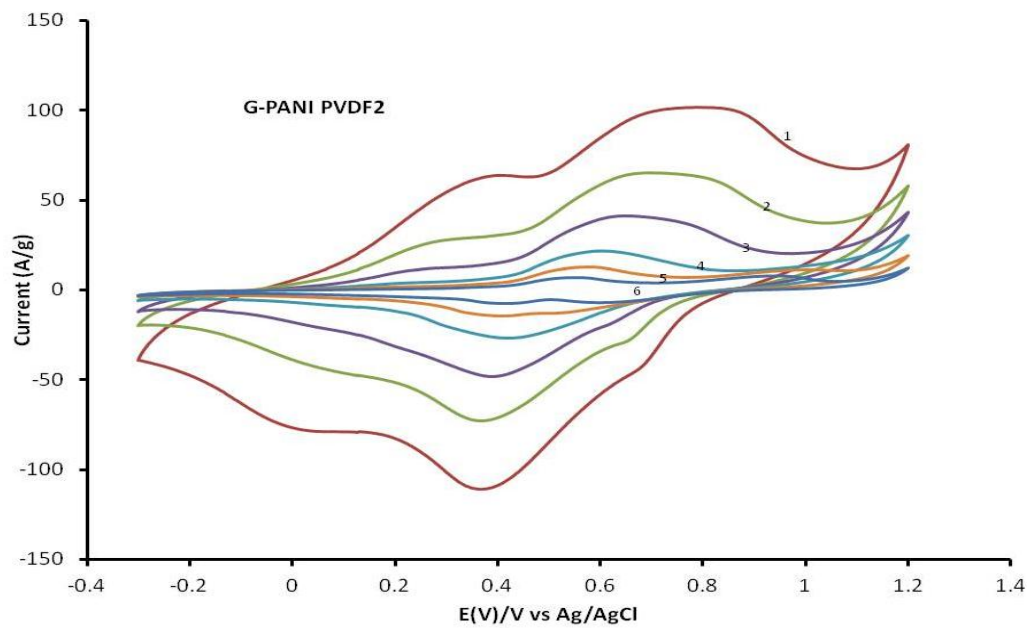
Figure 51: Cyclic voltammetry of G-PANI PVDF2 at different scan rates 1) 200 mV/sec, 2) 100 mV/sec, 3) 50 mV/sec, 4) 20 mV/sec, 5) 10 mV/sec and 6) 5 mV/sec
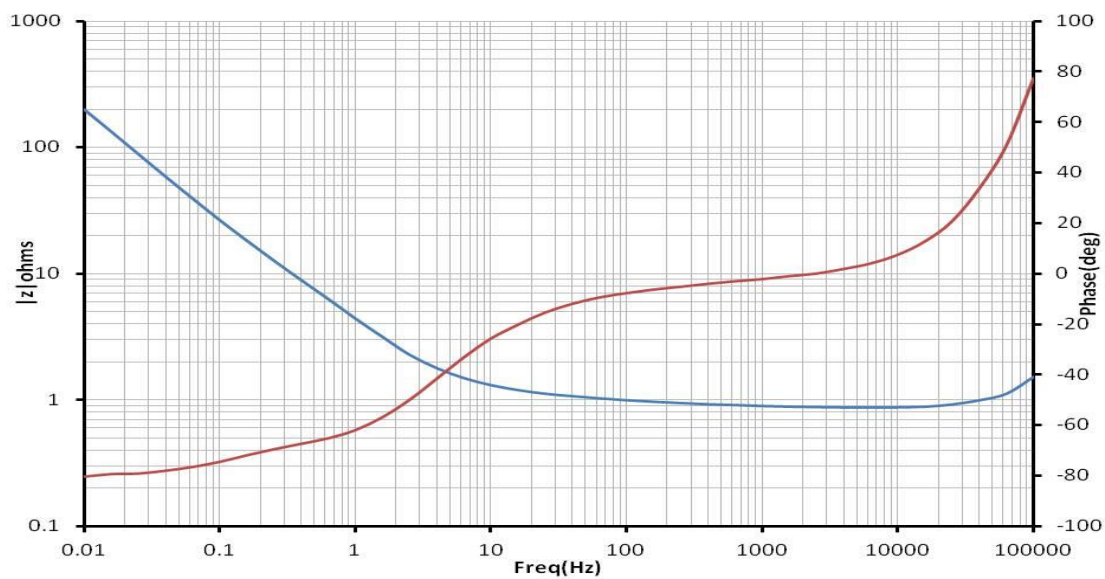
Figure 52: Bode plot of G-PANI PVDF2

66
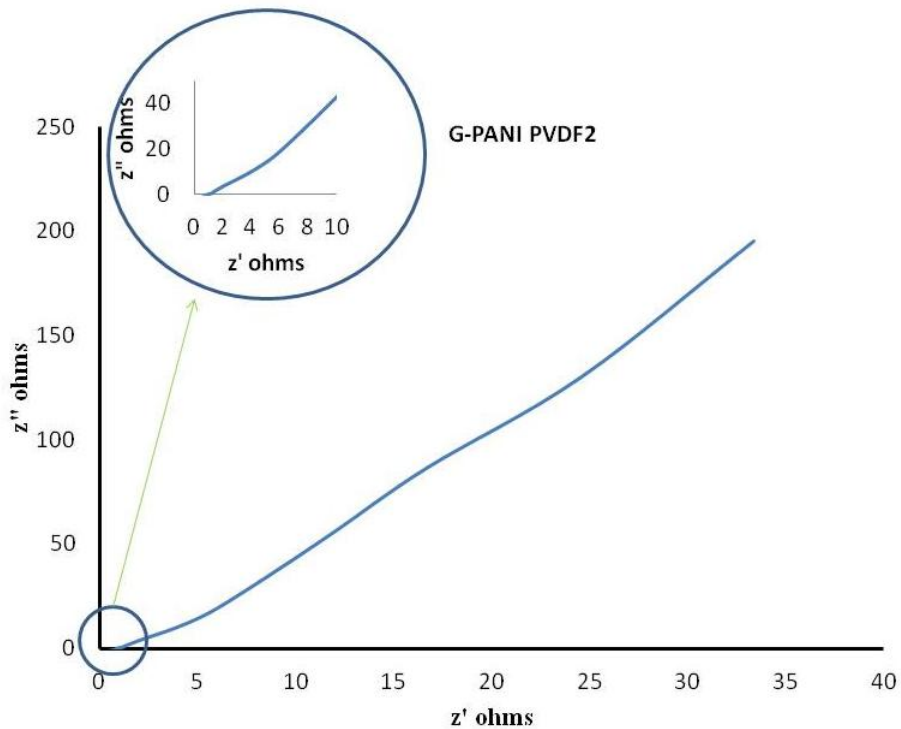
Figure 53: Nyquist plot of G-PANI PVDF2

Bode and Nyquist plots are extracted from the EIS measurement done at open circuit potential. Nice capacitive behavior as shown in figure (52) and (53) is observed in this case too, suggesting PVDF of 2 layers contributed to the G-PANI nanocomposite. The semi circle at the high frequency depicts the diffusion controlled system. The frequency range from 100 kHz to 0.01 Hz is taken to interpret the solution resistance, capacitive behavior and leakage resistance. The solution resistance is observed to be very minimum, suggesting very good power density value for the electrode material.
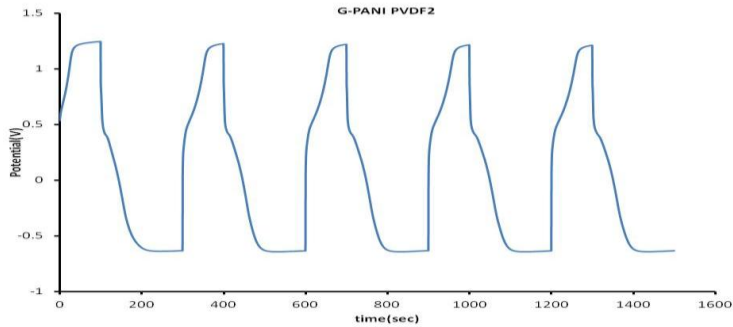
Figure 54: Charge discharge curves for G-PANI PVDF2 at 1 mA charging and discharging currents
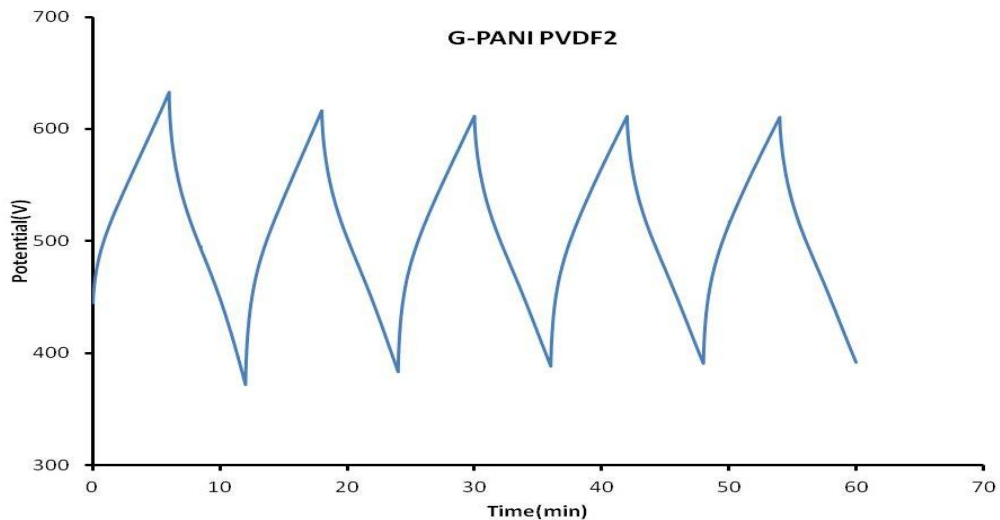
Figure 55: Charge discharge curves for G-PANI PVDF2 at 0.1mA charging and discharging currents

A very nice profile of charge-discharge curves as shown in figures (54) and (55) are seen to understand the rate of charging and discharging of G-PANI PVDF2. These curves suggest good energy density and power density values, along with high specific

capacitance values. Further analysis can give a better picture of performance for G-PANI

PVDF2 as a supercapacitor electrode material.

4.8 Self Leakage Measurement

Table 11: Area and mass specifications of samples for self leakage experiment

Sample	Area (cm^2)	Mass (mg)
G-PANI	1.17	0.94
G-PANI PVDF	1.7	1.5
G-PANI PVDF2	1.7	0.9
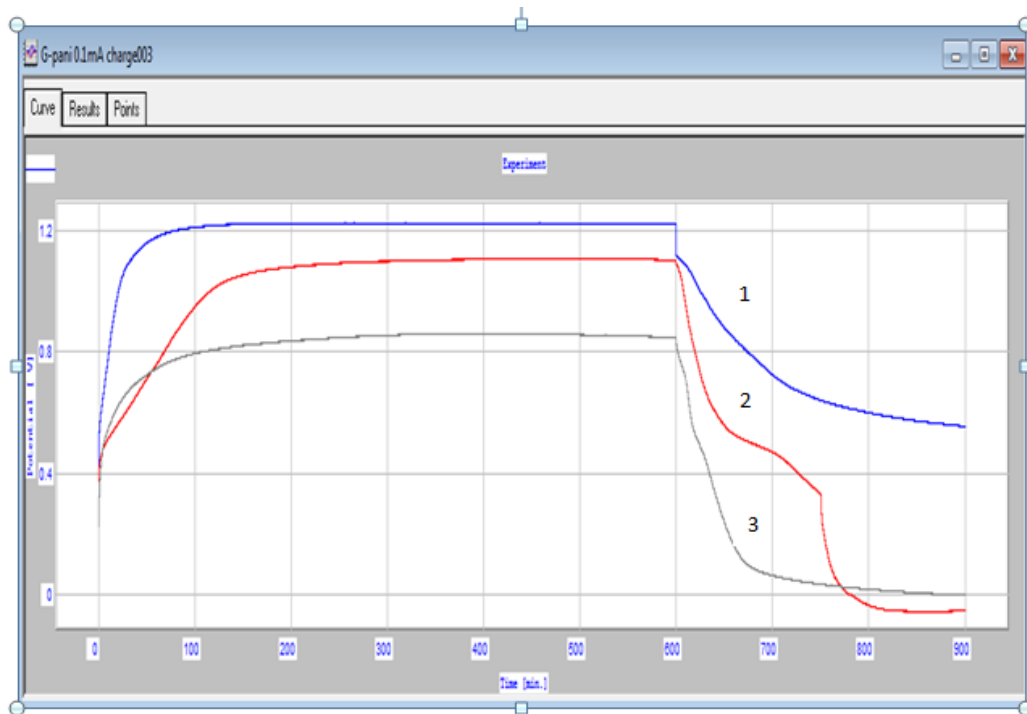
Figure 56: Discharging profile at open circuit potential for 1) G-PANI, 2) G-PANI PVDF and 3) G-PANI PVDF2

The self leakage experiment is done to understand the behavior of the system in aspect of

leakage current. The electrode material is charged to the maximum extent, attaining the

69

highest rated potential for about 10 hrs. It is then discharged by applying zero current to the cell. The voltage change with respect to time is taken at open circuit potential. The discharge profile gives intuition regarding leakage effect in supercapacitor. The change in potential is measured after 5 hrs, and discharging time is kept constant for all the samples for comparison purposes. From figure (56), it is seen that G-PANI showed continuous discharge profile and within 5 hours it reached from rated voltage 1.2V to 0.55V, almost reaching half of the rated voltage. G-PANI PVDF decreased from 1.1V to 0V within 5 hours time, and G-PANI PVDF2 decreased from 0.85V to 0V in the same time period. This clearly shows a lot of effort is required to conduct a lot more experiments on these samples using different electrolyte and molar concentrations to understand the behavior of self leakage. The experiment clearly proves that on application of PVDF on the G-PANI nanocomposite, there is a different discharging profile existing indicating the presence and role of PVDF monolayer on electrode material.

We see that, on application of PVDF layer on G-PANI of 1 layer or 2 layers, is not very useful in limiting the self leakage current associated with supercapacitor. One good approach is to increase the number of layers, so as to see the change in self leakage current at the same time retaining the capacitance value of G-PANI.

4.9 G-PANI PVDF (Multilayers)

The active surface area is around 1 cm^2 and the weight of G-PANI is considered around 0.1~0.5 mg. The CV measurements are done in 1M HCl electrolyte with Ag/AgCl reference electrode with symmetric configuration using same type of electrodes as work and counter electrodes. The CV curves at different scan rates for each type of electrode

materials are shown in the figures (57, 58, 59 & 60). The CV curves follow defined profile exhibiting the pseudocapacitive nature due to the redox reactions taking place at the electrode/electrolyte interface in a diffusion controlled environment. 1M HCl is a good conducting electrolyte resulting in high specific capacitance values to the electrode materials. The PVDF layers on G-PANI nanocomposite are horizontally deposited using the LB technique as Langmuir Schaefer films. The deposition of molecular sized monolayers proved to be effective for supercapacitor application. The specific capacitance is observed to be good enough for energy storage devices. This provides a scope to enhance the supercapacitor behavior by decreasing the self leakage current associated with the electrode material by depositing more than 2 layers of PVDF. A design to optimize the number of layers deposited on G-PANI will be helpful to understand and calculate the self leakage current associated with each electrode. Future work on this project could include optimization in number of PVDF monolayers on G-PANI nanocomposite to reduce the leakage current at the same instance retaining or improving the specific capacitance of the electrode material. As a part of the study, different layers of PVDF are deposited on G-PANI nanocomposite and CV measurements are done to understand the behavior of each type. CV curves of each type exhibited distinct profile deviations which might be due to the varied number of monolayers of PVDF present. They proved to be useful on application; they did not degrade the material performance and hence further research can be done to conduct the self leakage experiment to analyze the leakage effect. Moreover, such type of samples might give more intuition or information regarding the intermediate states in between the

71

oxidation and reduction states of polyaniline. This might be a very good study to understand the conducting polymer behavior in more detailed structure.

Figure 57: The CV of G-PANI PVDF2 as working electrode and counter electrode in 1M HCl where Ag/AgCl is the reference electrode at 1) 200 mV/sec, 2) 100 mV/sec, 3) 50 mV/sec, 4) 20 mV/sec, 5) 10 mV/sec and 6) 5 mV/sec.

Figure 58: The CV of G-PANI PVDF3 as working electrode and counter electrode in 1M HCl where Ag/AgCl is the reference electrode for different scan rates 1) 200 mV/sec, 2) 100 mV/sec, 3) 50 mV/sec, 4) 20 mV/sec, 5) 10 mV/sec and 6) 5 mV/sec

Figure 59: The CV of G-PANI PVDF5 as working electrode and counter electrode in 1M HCl where Ag/AgCl is the reference electrode for different scan rates 1) 200 mV/sec, 2) 100 mV/sec, 3) 50 mV/sec 4) 10 mV/sec and 5) 5 mV/sec

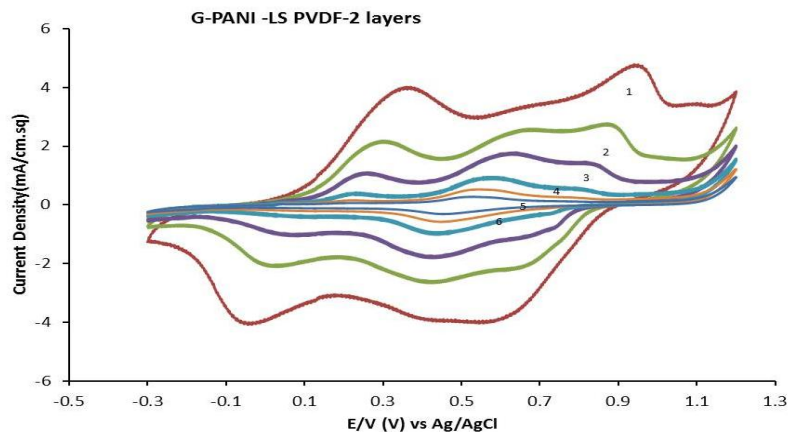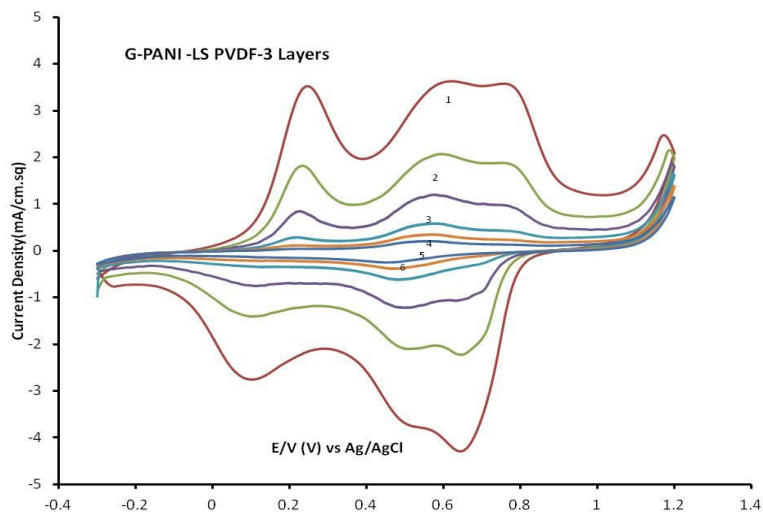*Figure 60: The CV of G-PANI PVDF6 as working electrode and counter electrode in 1M HCl where Ag/AgCl is the reference electrode for different scan rates 1) 200 mV/sec, 2) 100 mV/sec, 3) 50 mV/sec, 4) 20 mV/sec, 5) 10 mV/sec and 6) 5 mV/sec*
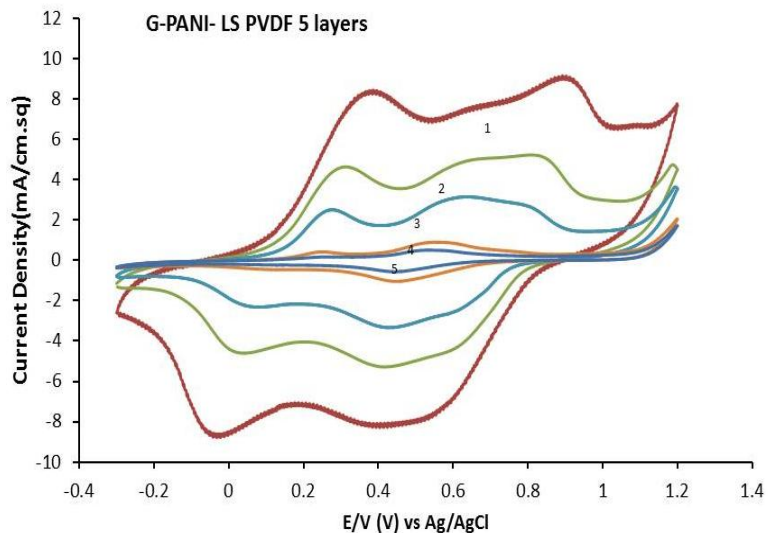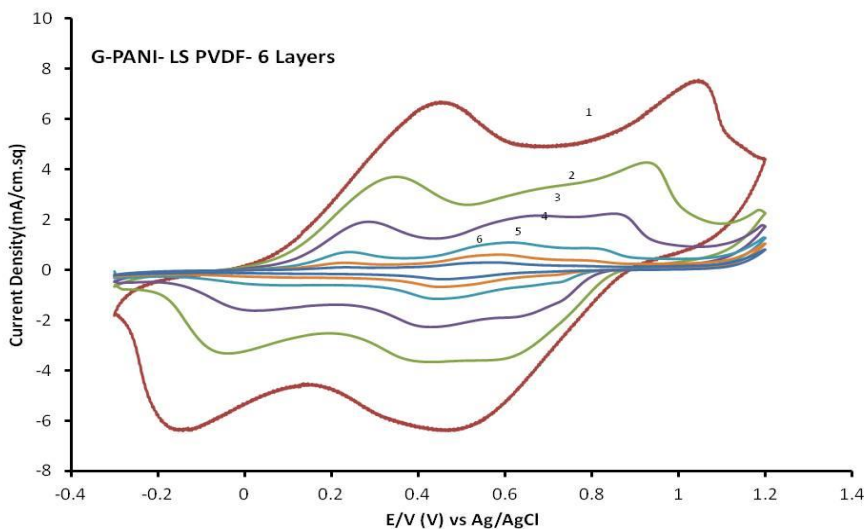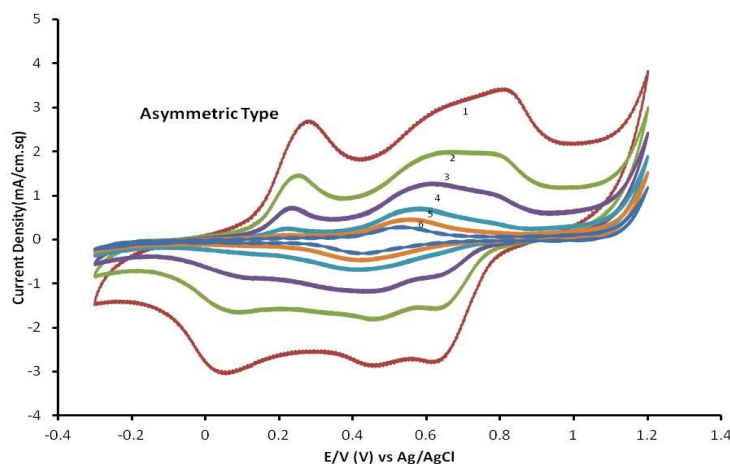
Figure 61: The CV of G-PANI with 2 layers of PVDF (LS) as working electrode in 1M HCl where Ag/AgCl is the reference electrode and G-PANI with 3 layers of PVDF (LB) as counter electrode for different scan rate (1) 200 mV/s (2) 100 mV/s (3) 50 mV/s (4) 20 mV/s (5) 10 mV/s and (6) 5 mV/s

The electrochemical cell was designed with the work electrode and counter electrode made up of different layers of PVDF on G-PANI nanocomposite to understand the asymmetric nature of a supercapacitor. G-PANI nanocomposite with 2 monolayers of PVDF (LS) films is taken as the work electrode and G-PANI with 3 Layers of PVDF (LB) films is taken as the counter electrode. The cell configuration is maintained the same for comparison purposes. The 1M HCl of high conductivity is a suitable electrolyte for high material performance in terms of capacitance and high energy density. The voltage limits are set from -0.3V to 1.2V and potential sweep at different scan rates is done to understand the change of current flow in the electrode at different instances of potential. The profile in figure (61) indicates excellent pseudocapacitance effect due to the role of faradic redox mechanisms undergoing at the electrode/electrolyte interface. This is due to the polyaniline, a highly conducting polymer, and due to the effect of the

74

monolayers of PVDF, which is electrochemically active. This clearly shows that any number of PVDF monolayers deposited using either LS or LB deposition can be used as electrode material, and asymmetric configuration consisting of different number of monolayers deposited in two ways can be used as the work and counter electrodes. Such asymmetric supercapacitors are very important to study the effect of overall capacitance of the electrochemical cell involving different types of electrodes. These supercapacitors perform differently from regular symmetric type due to their imbibed nature of two different types. These might give better capacitance values along with good energy density and power density ranges.

CHAPTER 5: CHARACTERIZATION USING DIFFERENT SPECTROSCOPY METHODS

5.1 Scanning Electron Microscopy (SEM)

The SEM images of GPANI (left) and GPANI PVDF (right) films coated on graphite substrates are shown in figure (62). The SEM images of graphene shows the flake like structure along with a very porous structure of the nanocomposite consisting of polyaniline (PANI). The SEM images of G-PANI PVDF in figure (62) represent the enhanced area for monolayer deposited PVDF.
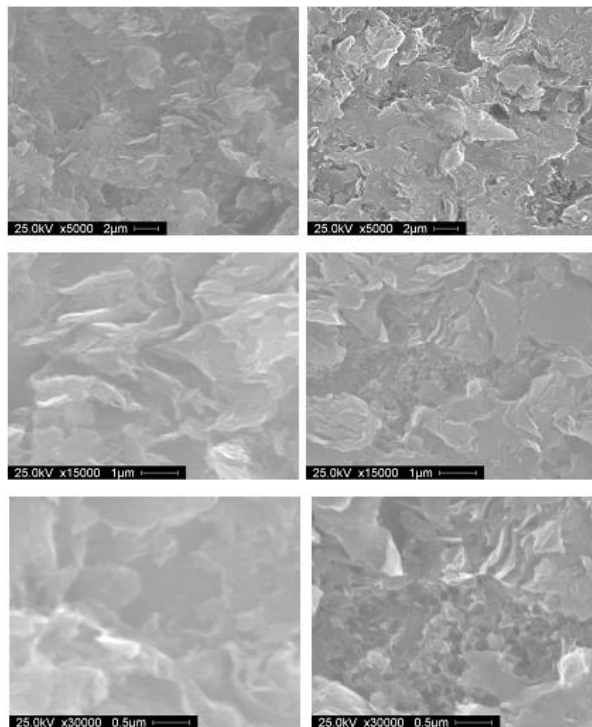
Figure 62: SEM images for G-PANI (left) and G-PANI PVDF (right)

The PVDF structure on graphite has also been studied using SEM pictures. Figure 63 shows the SEM images of PVDF on graphite substrate. We also see the distinguished film of PVDF enhancing the surface area of graphite. This also reveals the presence of PVDF monolayer on graphite substrate.
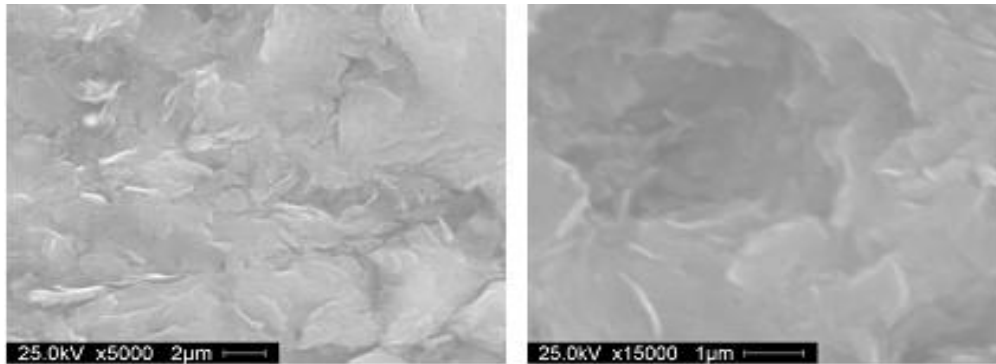
Figure 63: SEM images for PVDF on Graphite

5.2 Atomic Force Microscopy (AFM)

| (a) | (b) |
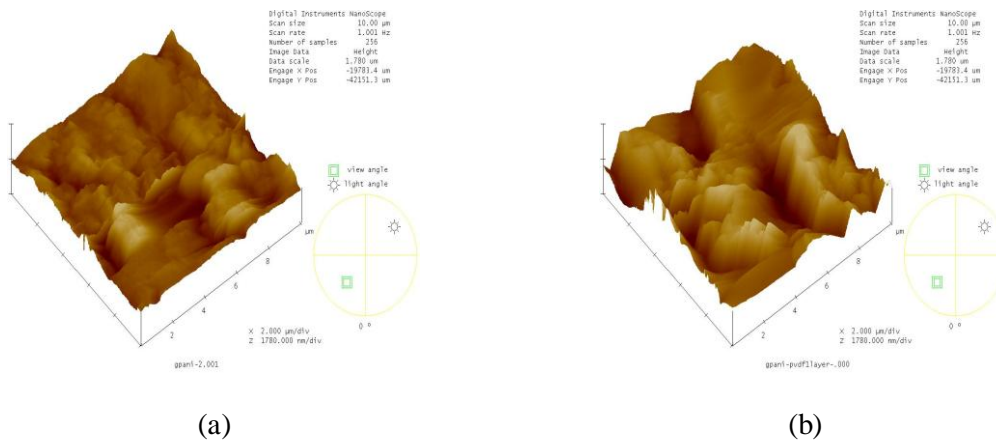
Figure 64: AFM images for (a) G-PANI and (b) G-PANI PVDF

The mean roughness measured for G-PANI is 116 nm where as for G-PANI PVDF it is 391.22nm. The mean roughness increased due to high surface area. Figure 64 (a) and (b) shows the AFM images for G-PANI and G-PANI PVDF films.

5.3 Ultra Violet Visible Spectroscopy

UV confirms the presence of PVDF monolayer on G-PANI nanocomposite. The sample with 1 layer of PVDF show less absorbance level compared to the sample with 3 layers of PVDF. As the number of layers increase, absorbance level also increases as shown in figure (65).
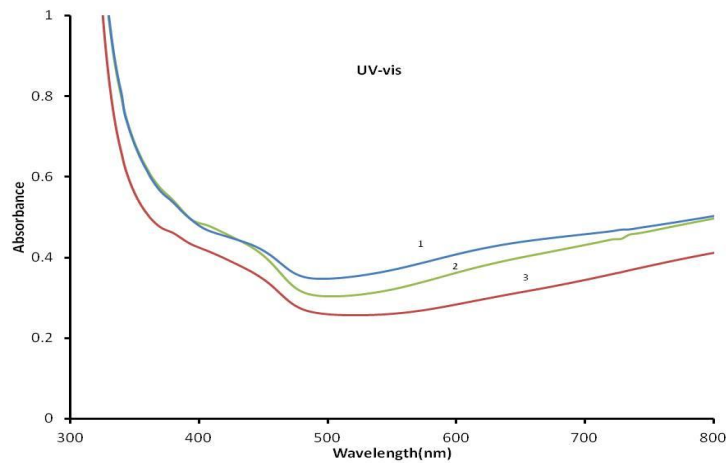
Figure 65: UV-vis for 1) G-PANI PVDF3, 2) G-PANI PVDF2, and 3) G-PANI PVDF

CHAPTER 6: CONCLUSIONS

The thin dielectric monolayer PVDF is used to understand the specific capacitance and leakage current of a supercapacitor. The LS monolayer/multilayers film of PVDF was deposited over G-PANI electrode to understand the properties of the fabricated supercapacitor. The G-PANI based supercapacitor reveals high specific capacitance in aqueous based electrolytes (example: HCl). The application of thin dielectric dipole aligned monolayer of PVDF on G-PANI has been shown to increase surface area of the electrode thus enhancing the specific capacitance of the supercapacitor. This supercapacitor configuration based on PVDF (prime layer) G-PANI and G-PANI PVDF has provided higher specific capacitance compared to G-PANI. However, the PVDF as a prime layer on graphite electrode has not shown any appreciable change in the electrochemical properties or an increase in the average capacitance. The LS film of PVDF on G-PANI has not shown the minimization of leakage current but revealed an increase in the specific capacitance due to enhancement in surface area associated with application of PVDF monolayer LS film. The Langmuir monolayer/multilayer PVDF film has also shown the control of redox properties of G-polyaniline film. The PVDF has also shown the defined closed cyclic voltammetric hysteresis curve similar to redox material. The increase of specific capacitance could also be due to the electrochemical properties of PVDF film. The specific capacitance values obtained from cyclic voltammetry for G-PANI and G-PANI PVDF in presence of PVDF monolayer on G-PANI nanocomposite have been found to be nearly twice than the G-PANI film. The self-

79

leakage tests were conducted on supercapacitors consisted of one monolayer and two monolayers of G-PANI PVDF and G-PANI electrodes. The application of one or two monolayers of PVDF has not shown the minimization of leakage related to uniformity of the film. The equivalent circuit has been drawn based on electrochemical properties to understand the double layer capacitor based on G-PANI PVDF and G-PANI based electrodes. Future scope could include optimization in the number of layers of PVDF on top of the G-PANI based electrode or application of real dielectric polymer (polyimide) or metal oxide (barium strontium titanate), so that the self leakage could be reduced and at the same time maintaining desired level of specific capacitance of the supercapacitor.

REFERENCES

[1]   B. E. Conway and W. G. Pell, "Double-layer and pseudocapacitance types of electrochemical capacitors and their applications to the development of hybrid devices," *Journal of Solid State Electrochemistry*, vol. 7, no. 9, pp. 637–644, 2003.

[2]   M.Jayalakshmi and K.Balasubramanian, "Simple Capacitors to Supercapacitors-An Overview," *Journal of Electrochemical Science*, vol. 3, no. 11, pp. 1196–1217, 2008.

[3]   "Application Note: Testing Electrochemical Capacitors Part1- Cyclic voltammetry and Leakage current," *www.gamry.com*. [Online]. Available: http://www.gamry.com/assets/Application-Notes/Testing-Super-Capacitors-Pt1.pdf.

[4]   Marin S. Halper and James C.Ellenbogen, "Supercapacitors : A Brief Overview." [Online]. Available: http://www.mitre.org/work/tech_papers/tech_papers_06/06_0667/06_0667.pdf.

[5]   A. Yu, A. Davies, and Z. Chen, "Electrochemical Supercapacitors," in *Electrochemical Technologies for Energy Storage and Conversion*, R.-S. Liu, L. Zhang, X. Sun, H. Liu, and J. Zhang, Eds. Wiley-VCH Verlag GmbH & Co. KGaA, 2011, pp. 317–382.

[6]   N. A. Choudhury, S. Sampath, and A. K. Shukla, "Hydrogel-polymer electrolytes for electrochemical capacitors: an overview," *Energy Environ. Sci.*, vol. 2, no. 1, pp. 55–67, Dec. 2008.

[7]   Prashanth Jampani, A.Manivannan, and Prashant N.Kumta, "Advancing the supercapacitor materials and technology frontier for improving power quality," *The Electrochemical Society Interface*, pp. 57–62, 2010.

[8]   "Wasted Energy Topics on Energy,Resources, waste and culture," *wastedenergy.net*. [Online]. Available: http://wastedenergy.net/category/energy-production/.

[9]   Y. Diab, P. Venet, H. Gualous, and G. Rojat, "Self-Discharge Characterization and Modeling of Electrochemical Capacitor Used for Power Electronics Applications," *IEEE Transactions on Power Electronics*, vol. 24, no. 2, pp. 510–517, Feb.

[10]   "self discharge," *www.garmanage.com*. [Online]. Available: http://www.garmanage.com/atelier/index.cgi?path=public/Energy_storage/Supercapacitors/Properties/Selfdischarge.

[11]   "Application Note Testing Electrochemical Capacitors Part3- Electrochemical Impedance Spectroscopy," *www.gamry.com*. [Online]. Available: http://www.gamry.com/assets/Application-Notes/Testing-Super-Capacitors-Pt3.pdf.

[12]   H. El Brouji, J.-M. Vinassa, O. Briat, N. Bertrand, and E. Woirgard, "Ultracapacitors self discharge modelling using a physical description of porous electrode impedance," in *IEEE Vehicle Power and Propulsion Conference, 2008. VPPC '08*, Sept., pp. 1–6.

[13]   B. E. Conway, V. Birss, and J. Wojtowicz, "The role and utilization of pseudocapacitance for energy storage by supercapacitors," *Journal of Power Sources*, vol. 66, no. 1–2, pp. 1–14, May 1997.

[14]   "Application note: Maxwell Technologies' Test Procedures for capacitance, ESR, Leakage current and Self Discharge Characterizations of Ultracapacitors," *www.maxwell.com*. [Online]. Available: http://www.maxwell.com/products/ultracapacitors/docs/applicationnote_maxwelltest procedures.pdf.

[15]   Kuldeep and Bharati Dwivedi, "Supercapacitor energy storage system for power quality improvement : An overview," *Journal of electrical systems*, vol. 5, no. 4, Dec. 2009.

[16]   Bobby Maher, "Ultracapacitors and the Hybrid Electric Vehicle," *The Alternative Energy eMagazine*.

[17]   Chijuan Hu, "Fluid coke derived Activated Carbon as Electrode Material for Electrochemical Double Layer Capacitor." www.sensorprod.com.

[18]   I. Hadjipaschalis, A. Poullikkas, and V. Efthimiou, "Overview of current and future energy storage technologies for electric power applications," *Renewable and Sustainable Energy Reviews*, vol. 13, no. 6–7, pp. 1513–1522, Aug. 2009.

[19]   M. R.-V. Z Stević, "Construction and Characterisation of Double Layer Capacitors," vol. 1175050, 2010.

[20]   Y. Zhang, H. Feng, X. Wu, L. Wang, A. Zhang, T. Xia, H. Dong, X. Li, and L. Zhang, "Progress of electrochemical capacitor electrode materials: A review," *International Journal of Hydrogen Energy*, vol. 34, no. 11, pp. 4889–4899, Jun. 2009.

[21]   M. D. Stoller and R. S. Ruoff, "Best practice methods for determining an electrode material's performance for ultracapacitors," *Energy Environ. Sci.*, vol. 3, no. 9, pp. 1294–1301, Aug. 2010.

[22]   *School of Chemistry and Physics, University of Adelaide*. [Online]. Available: http://www.chemistry.adelaide.edu.au/external/soc-rel/content/cv.htm.

[23]   "Application Note: Testing Electrochemical capacitors Part-2 Cyclic charge Discharge and stacks," *www.gamry.com*. [Online]. Available: http://www.gamry.com/assets/Application-Notes/Testing-Super-Capacitors-Pt3.pdf.

[24]   "Application Note Equivalent Circuit Modeling in EIS," *www.gamry.com*. [Online]. Available: http://www.gamry.com/assets/Application-Notes/Equivalent-Circuit-Modeling-in-EIS.pdf.

[25]   "Application note Basics of Electrochemical Impedance Spectroscopy," *www.gamry.com*. [Online]. Available: http://www.gamry.com/assets/Application-Notes/Basics-of-EIS.pdf.

[26]   C. Liu, Z. Yu, D. Neff, A. Zhamu, and B. Z. Jang, "Graphene-Based Supercapacitor with an Ultrahigh Energy Density," *Nano Lett.*, vol. 10, no. 12, pp. 4863–4868, Dec. 2010.

[27]   Y. Wang, Z. Shi, Y. Huang, Y. Ma, C. Wang, M. Chen, and Y. Chen, "Supercapacitor Devices Based on Graphene Materials," *J. Phys. Chem. C*, vol. 113, no. 30, pp. 13103–13107, Jul. 2009.

[28]   M. D. Stoller, S. Park, Y. Zhu, J. An, and R. S. Ruoff, "Graphene-Based Ultracapacitors," *Nano Lett.*, vol. 8, no. 10, pp. 3498–3502, Oct. 2008.

[29]   F. Alvi, "Graphene–polyethylenedioxythiophene conducting polymer nanocomposite based supercapacitor," *Electrochimica Acta*, vol. 56, no. 25, pp. 9406–9412, Oct. 2011.

[30]   F. B. Alvi, "Graphene-polythiophene nanocomposite as novel supercapacitor electrode material," *Journal of New Materials for Electrochemical Systems*, vol. 15, no. 2, pp. 89–95, 2012.

[31]   F. Alvi, M. K. Ram, P. Basnayaka, E. Stefanakos, Y. Goswami, A. Hoff, and A. Kumar, "Electrochemical Supercapacitors Based on Graphene-Conducting Polythiophenes Nanocomposite," *ECS Trans.*, vol. 35, no. 34, pp. 167–174, Oct. 2011.

[32]   J. An, J. Liu, Y. Zhou, H. Zhao, Y. Ma, M. Li, M. Yu, and S. Li, "Polyaniline-Grafted Graphene Hybrid with Amide Groups and Its Use in Supercapacitors," *J. Phys. Chem. C*, vol. 116, no. 37, pp. 19699–19708, Sep. 2012.

[33]   P. A. Basnayaka, M. K. Ram, E. K. Stefanakos, and A. Kumar, "Supercapacitors based on graphene–polyaniline derivative nanocomposite electrode materials," *Electrochimica Acta*, vol. 92, pp. 376–382, Mar. 2013.

[34]   P. A. Basnayaka, F. Alvi, M. K. Ram, R. Tufts, and A. Kumar, "A Comparative Study on Substituted Polyanilines for Supercapacitors," *MRS Online Proceedings Library*, vol. 1388, p. null–null, 2012.

[35]   J. Yan, T. Wei, B. Shao, Z. Fan, W. Qian, M. Zhang, and F. Wei, "Preparation of a graphene nanosheet/polyaniline composite with high specific capacitance," *Carbon*, vol. 48, no. 2, pp. 487–493, Feb. 2010.

[36]   K. Zhang, L. L. Zhang, X. S. Zhao, and J. Wu, "Graphene/Polyaniline Nanofiber Composites as Supercapacitor Electrodes," *Chem. Mater.*, vol. 22, no. 4, pp. 1392–1401, Feb. 2010.

[37]   H. Gómez, M. K. Ram, F. Alvi, P. Villalba, E. (Lee) Stefanakos, and A. Kumar, "Graphene-conducting polymer nanocomposite as novel electrode for supercapacitors," *Journal of Power Sources*, vol. 196, no. 8, pp. 4102–4108, Apr. 2011.

[38]   H. Gomez, F. Alvi, P. Villalba, M. K. Ram, and A. Kumar, "Supercapacitor Based on Graphene – Polyaniline Nanocomposite Electrode," *MRS Online Proceedings Library*, vol. 1312, p. null–null, 2011.

[39]   I. Y. Sapurina and M. A. Shishov, "Oxidative Polymerization of Aniline: Molecular Synthesis of Polyaniline and the Formation of Supramolecular Structures," in *New Polymers for Special Applications*, A. De Souza Gomes, Ed. InTech, 2012.

[40]   S. A. Ketkar, M. Ram, A. Kumar, T. Weller, and A. M. Hoff, "Comparative Study of Electrode Stabilization Technique for Graphene-Polyaniline Nanocomposite Electrodes Using Dielectrics for Supercapacitor Applications," *Meet. Abstr.*, vol. MA2012–02, no. 6, pp. 591–591, Jun. 2012.

[41]   S. Ketkar, M. K. Ram, A. Kumar, T. Weller, and A. Hoff, "Electrical and Structural Diagnostics of Barium Strontium Titanate (BST) Thin Films," *MRS Online Proceedings Library*, vol. 1292, p. null–null, 2011.

[42]   "Ferroelectric polymers," *Wikipedia, the free encyclopedia*. 18-Feb-2013.

[43]   D. Damjanovic, "Ferroelectric, dielectric and piezoelectric properties of ferroelectric thin films and ceramics," *Rep. Prog. Phys.*, vol. 61, no. 9, p. 1267, Sep. 1998.

[44]   H. L. W. Chan, "Smart ferroelectric materials for sensors and mechatronic device applications," in *Electron Devices Meeting, 1999. Proceedings. 1999 IEEE Hong Kong*, pp. 68–71.

[45]   Y. C. Shu and K. Bhattacharya, "Domain patterns and macroscopic behaviour of ferroelectric materials," *Philosophical Magazine Part B*, vol. 81, no. 12, pp. 2021–2054, 2001.

[46]   "Ferroelectricity," *Wikipedia, the free encyclopedia*. 06-Feb-2013.

[47]   "Polyvinylidene fluoride," *Wikipedia, the free encyclopedia*. 02-Mar-2013.

[48]   Z.-Y. Wang, H.-Q. Fan, K.-H. Su, and Z.-Y. Wen, "Structure and piezoelectric properties of poly(vinylidene fluoride) studied by density functional theory," *Polymer*, vol. 47, no. 23, pp. 7988–7996, Oct. 2006.

[49]   T. Mirfakhrai, J. D. W. Madden, and R. H. Baughman, "Polymer artificial muscles," *Materials Today*, vol. 10, no. 4, pp. 30–38, Apr. 2007.

[50]   Y. JIANG, Y. YE, J. YU, Y. YANG, J. XU, and Z. WU, "A Study on Ferroelectric Pvdf Ultrathin Films Prepared by Lb Technique," *Integrated Ferroelectrics*, vol. 88, no. 1, pp. 21–26, 2007.

[51]   "Piezoelectric polymers." [Online]. Available: http://www.physics.montana.edu/eam/polymers/piezopoly.htm.

[52]   R. Tadros-Morgane and H. Kliem, "Polarization curves of Langmuir–Blodgett PVDF-copolymer films," *Journal of Physics D: Applied Physics*, vol. 39, no. 22, pp. 4872–4877, Nov. 2006.

[53]   E. Y. Tsymbal, "APPLIED PHYSICS: Tunneling Across a Ferroelectric," *Science*, vol. 313, no. 5784, pp. 181–183, Jul. 2006.

[54]   S. Chen, K. Yao, F. E. H. Tay, and L. L. S. Chew, "Comparative investigation of the structure and properties of ferroelectric poly(vinylidene fluoride) and poly(vinylidene fluoride-trifluoroethylene) thin films crystallized on substrates," *Journal of Applied Polymer Science*, p. NA–NA, 2010.

[55]   W.-C. Chen, T.-C. Wen, and H. Teng, "Polyaniline-deposited porous carbon electrode for supercapacitor," *Electrochimica Acta*, vol. 48, no. 6, pp. 641–649, Feb. 2003.

[56]   C. Lei, P. Wilson, and C. Lekakou, "Effect of poly(3,4-ethylenedioxythiophene) (PEDOT) in carbon-based composite electrodes for electrochemical supercapacitors," *Journal of Power Sources*, vol. 196, no. 18, pp. 7823–7827, Sep. 2011.

[57]   W. Lu, R. Hartman, L. Qu, and L. Dai, "Nanocomposite Electrodes for High-Performance Supercapacitors," *J. Phys. Chem. Lett.*, vol. 2, no. 6, pp. 655–660, Mar. 2011.

[58]   S. Ducharme, "An Inside-Out Approach to Storing Electrostatic Energy," *ACS Nano*, vol. 3, no. 9, pp. 2447–2450, Sep. 2009.

[59]   Y. C. Li, S. C. Tjong, and R. K. Y. Li, "Electrical conductivity and dielectric response of poly(vinylidene fluoride)–graphite nanoplatelet composites," *Synthetic Metals*, vol. 160, no. 17–18, pp. 1912–1919, Sep. 2010.

[60]   S. Chen, X. Li, K. Yao, F. E. H. Tay, A. Kumar, and K. Zeng, "Self-polarized ferroelectric PVDF homopolymer ultra-thin films derived from Langmuir–Blodgett deposition," *Polymer*, vol. 53, no. 6, pp. 1404–1408, Mar. 2012.

[61]   S. A. Hussain, "Langmuir-Blodgett Films a unique tool for molecular electronics," *arXiv:0908.1814*, Aug. 2009.

[62]   G. G. Roberts, "An applied science perspective of Langmuir-Blodgett films," *Advances in Physics*, vol. 34, no. 4, pp. 475–512, 1985.

[63]   Antonella Badia, "Langmuir and Langmuir-Blodgett Film Assemblies."

[64]   M. C. Petty, *Langmuir-Blodgett Films: An Introduction*. Cambridge University Press, 1996.

[65]   "ZsimpWin," *Princeton Applied Research*. [Online]. Available: http://www.princetonappliedresearch.com/Our-Products/Electrochemical-Software/ZSimpWin.aspx.

APPENDICES

Appendix A Copyright and Permissions

A.1 Permission to Modify Figure 2

USF

Venkata Priyanka Bolisetty <venkatapriya@mail.usf.edu>

Requesting Permission to reuse Figure published in article for Thesis Submission

Nurul Choudhury <nachoudhury@gmail.com>   Thu, Mar 7, 2013 at 12:01 PM
To: Venkata Priyanka Bolisetty <venkatapriya@mail.usf.edu>

Dear Priyanka,

The copy right of the article has been transferred to the Publisher. So, the authors do not have any right to give permission. However, you can use the figure with a litte modification in it.

Best wishes,
Nurul.

On Wed, Mar 6, 2013 at 6:27 PM, Venkata Priyanka Bolisetty <venkatapriya@mail.usf.edu> wrote:
> Dear Choudhury,
>
> I am Venkata Priyanka Bolisetty, Graduate Research Student from University of South Florida. I am going to submit my thesis as part of my graduate coursework on " **Novel Approach of using Polyvinylidene Fluoride**
>
> **Langmuir -Schaefer film on Graphene-Polyaniline nanocomposite for Supercapacitor Applications**". I would like to use one of the figures in the article mentioned below. So, When I try to take permission, it was
>
> costing me 144 USD, which is very huge amount for me to afford. I Would like to take your permission to go ahead and use the figure with your consent, if it is not possible, can you provide me with a similar picture , where I
>
> can reuse it for my thesis. The details of the figure are mentioned below.
>
> Please kindly help me out with this.
>
> Looking Forward to hear from you,
>
>
> Thanks
>
> Priyanka
>
>
> Article :
> **Hydrogel-polymer electrolytes for electrochemical capacitors: an overview**
> N. A. Choudhury,a S. Sampathb and A. K. Shukla*ac
> Received 1st July 2008, Accepted 24th October 2008
> First published as an Advance Article on the web 1st December 2008
> DOI: 10.1039/b811217g
>
> Publisher : Energy and Environmental science
> Volume :2
> Issue : 1
> Pages : 55-67
>
> Figure : 1 , Page 56 Figure name: A Ragone plot comparison of power and energy densities for
> electrochemical capacitors, storage batteries and fuel cells.

--
Nurul A. Choudhury
Postdoctoral Research Fellow
Department of Chemistry
Queen's University
Chernoff Hall, Room No. 531
90 Bader Lane
Kingston, Ontario, Canada K7L 3N6
Tel: +1-613-533-6000, Extn. 75484
Fax: +1-613-533-6669
Email: choudhuryn@chem.queensu.ca

Appendix A (continued)

A.2 Permission to Reprint Figure 9

Appendix A (continued)

A.3 Permission to Reprint Figure 11

RightsLink — Copyright Clearance Center

Thank You For Your Order!

Dear Miss. Venkata Priyanka Bolisetty,

Thank you for placing your order through Copyright Clearance Center's RightsLink service. Elsevier has partnered with RightsLink to license its content. This notice is a confirmation that your order was successful.

Your order details and publisher terms and conditions are available by clicking the link below:
http://s100.copyright.com/CustomerAdmin/PLF.jsp?ref=7db31300-cd7e-42db-bc70-a3b4036f8583

Order Details
Licensee: Venkata Bolisetty
License Date: Mar 6, 2013
License Number: 3103300737296
Publication: Materials Today
Title: Polymer artificial muscles
Type Of Use: reuse in a thesis/dissertation
Total: 0.00 USD

To access your account, please visit https://myaccount.copyright.com.

Please note: Online payments are charged immediately after order confirmation; invoices are issued daily and are payable immediately upon receipt.

To ensure we are continuously improving our services, please take a moment to complete our customer satisfaction survey.

B.1:v4.2

+1-877-622-5543 / Tel: +1-978-646-2777
customercare@copyright.com
http://www.copyright.com